Journal of Food Biochemistry

WILEY

RESEARCH ARTICLE OPEN ACCESS

Hepatoprotective Effects of Cipollotto Nocerino Leaf Extract in HepG2 Cells: SIRT1-Mediated Regulation of Lipid Metabolism and Oxidative Stress

Maria Rosaria Miranda[1,2] | Giovanna Aquino[3] | Tania Ciaglia[1] | Giuseppina Amodio[4] | Manuela Giovanna Basilicata[5] | Mario Felice Tecce[1] | Vincenzo Vestuto[1] | Pietro Campiglia[1] | Michele Manfra[6] | Giacomo Pepe[1,7]

[1]Department of Pharmacy, University of Salerno, Fisciano, Italy | [2]Department of Medicine, Digestive Health Research Institute, Case Western Reserve University School of Medicine, Cleveland, Ohio, USA | [3]AREA Science Park, Laboratorio Di Multi-Omica Area Sud (LAAS), Trieste, Italy | [4]Department of Medicine, Surgery and Dentistry "Scuola Medica Salernitana", University of Salerno, Baronissi, Italy | [5]Department of Advanced Medical and Surgical Sciences, University of Campania "Luigi Vanvitelli", Naples, Italy | [6]Department of Scienze della Salute, University of Basilicata, Potenza, Italy | [7]National Biodiversity Future Center (NBFC), Palermo, Italy

Correspondence: Manuela Giovanna Basilicata (manuelagiovanna.basilicata@unicampania.it) | Vincenzo Vestuto (vvestuto@unisa.it)

Received: 20 January 2026 | **Revised:** 20 April 2026 | **Accepted:** 26 April 2026

Academic Editor: Anupama Bose

ABSTRACT

Cipollotto Nocerino (*Allium cepa* L.), a Protected Designation of Origin (PDO) spring onion from the Campania region (Southern Italy), yields leaves that are a neglected agri-food by-product, typically discarded despite their rich phytochemical profile, and remain largely unexplored, particularly regarding their potential to counteract hepatic steatosis. This study evaluated the hepatoprotective activity of a CN leaf alcoholic extract in HepG2 cells exposed to oleic acid (OA) and palmitic acid (PA) to induce steatosis, in both two- and three-dimensional culture systems. UHPLC-HRMS/MS analysis revealed a complex phytochemical profile comprising polar and apolar lipids, chlorophylls, carotenoids, and flavonoids. These metabolites, known to regulate oxidative stress, inflammation, and lipid metabolism, likely mediate CN's protective effects against lipotoxicity. In HepG2 cells, CN markedly improved cell viability, attenuated lipid droplet accumulation, restored redox balance, alleviated endoplasmic reticulum (ER) stress, preserved mitochondrial membrane potential, and reduced inflammation markers. Sirtuin 1 (SIRT1) expression and activity were enhanced by CN in the presence of OA/PA, and the pharmacological modulation confirmed its partial involvement in these protective effects. These findings demonstrate that CN counteracts free fatty acid–induced lipotoxicity through an integrated mechanism targeting lipid metabolism, oxidative and ER stress, mitochondrial function, and inflammation, with SIRT1 activation acting as a central, although not exclusive, mediator supporting its potential as a promising, sustainable nutraceutical for the prevention or adjunct management of nonalcoholic fatty liver disease.

1 | Introduction

Nutraceuticals are recognized as bioactive compounds capable of modulating metabolic, oxidative, and inflammatory pathways, supporting the prevention and management of chronic diseases [1, 2]. Several natural compounds, including resveratrol, epigallocatechin gallate, and curcumin, have shown relevant antioxidant and metabolic regulatory effects in cardiometabolic and liver disorders [3–7]. In this context, the valorization of agro-industrial by-products, particularly in the Mediterranean area, has emerged as a sustainable strategy to obtain novel sources of bioactive molecules while reducing environmental impact [8–10].

Maria Rosaria Miranda and Giovanna Aquino are co-first authors.

Nonalcoholic fatty liver disease (NAFLD) is one of the most prevalent chronic liver disorders worldwide, closely associated with obesity, insulin resistance, and dyslipidemia [11]. Hepatic lipid accumulation in NAFLD is not limited to triglycerides but also involves bioactive lipid species such as free fatty acids (FFAs), diacylglycerols, ceramides, and cholesterol derivatives, whose qualitative composition critically influences disease progression. Excess circulating FFAs increased de novo lipogenesis, impaired mitochondrial β-oxidation, and defective very low–density lipoprotein (VLDL) export contribute to lipid overload and lipotoxicity. These alterations trigger a cascade of interconnected events, including mitochondrial dysfunction, oxidative stress, and ER stress, ultimately promoting inflammatory responses and hepatocellular injury. The interplay between lipid quality, subcellular compartmentalization, and stress signaling pathways is now recognized as a key determinant of the transition from simple steatosis to more severe forms of liver damage [11, 12]. In this context, plant-derived nutraceuticals, including silymarin, chlorogenic acid, berberine, and polyphenol-rich extracts, have shown the ability to attenuate lipid accumulation and restore redox and metabolic homeostasis in experimental models of steatosis [13].

Among the molecular targets of interest, sirtuin 1 (SIRT1), a NAD^+-dependent deacetylase, represents a particularly relevant target. SIRT1 regulates lipid catabolism, mitochondrial biogenesis, and cellular response to oxidative and ER stress. Its activation has been associated with decreased triglyceride deposition, improved antioxidant defenses, and suppression of nuclear factor kappa B (NF-κB)–mediated inflammation. Therefore, compounds that enhance SIRT1 activity are being investigated as potential strategies to limit hepatic fat accumulation and their downstream complications [14, 15].

CN is a traditional Italian spring onion (*A. cepa* L.) with Protected Designation of Origin (PDO) status, widely cultivated in the Campania region. While the edible bulb is the main commercial product, the aerial parts, particularly the leaves, are usually discarded, thus generating underutilized agricultural biomass. Unlike bulbs and dry skins, which have been extensively studied, CN leaves remain largely unexplored, representing a clear gap in the literature and a promising target for nutraceutical valorization [16, 17].

Leaves of *Allium* species are rich in phenolic compounds, flavonoids, and other secondary metabolites, often at levels comparable to or higher than those in bulbs. Several studies report that onion leaves contain high amounts of quercetin derivatives and display strong antioxidant activity, thus supporting their potential role in preventing oxidative stress–related disorders [18, 19].

The phytochemical and functional properties of CN leaves have only recently been explored. Our previous studies showed for the first time that microwave-assisted extraction yields leaf extracts with high total phenolic content (TFC) and strong antioxidant activity, and two-dimensional LC-MS analyses identified diverse bioactive compounds, including flavonoids, saponins, and FAs, supporting their potential as functional ingredients [10, 20]. The valorization of onion leaves aligns with circular economy and biorefinery principles by repurposing agricultural waste into high-value nutraceuticals. While similar approaches have been applied to other *Allium* by-products, such as onion skins and peels, since their residue remains both geographically and culturally specific, CN leaves are still poorly investigated despite their rich phytochemical profile [16]. Notably, no studies have yet evaluated the effects of CN leaf extracts in the context of NAFLD, nor their potential to modulate lipid metabolism and SIRT1-related pathways involved in steatosis progression.

To gain insights into the phytochemical composition of the CN extract and to identify classes of bioactive compounds potentially contributing to its protective effects against NAFLD, a comprehensive UHPLC-HRMS/MS analysis was performed. This approach enabled an in-depth characterization of the alcoholic extract, providing detailed information on its major constituents and molecular diversity. The extract was tested in HepG2 cells exposed to oleic acid (OA) and palmitic acid (PA) to induce diet-related steatosis, in both two-dimensional and three-dimensional culture systems. We assessed the ability of CN to attenuate lipid droplet accumulation, regulate genes involved in lipid metabolism and SIRT1 signaling, and enhance SIRT1 activity in the presence of FAs. In addition, we evaluated CN effects on oxidative stress, ER stress markers, mitochondrial membrane potential, inflammatory mediators, and cell injury. Finally, the contribution of SIRT1 was examined through pharmacological modulation using SIRT1 inhibitors and activators, confirming its central role in mediating the hepatoprotective effects of CN. Our findings highlight the capacity of CN to mitigate steatosis and related oxidative and inflammatory damage, supporting its development as a sustainable nutraceutical for the prevention of NAFLD.

2 | Materials and Methods

2.1 | Sample Preparation

CN leaves were kindly provided by the consortium for the protection of "Cipollotto Nocerino PDO" and originated from certified production areas in the Agro Nocerino-Sarnese (Campania, Italy). Samples were collected during the spring harvest season at commercial maturity, corresponding to the standard stage used for fresh consumption. After collecting, samples were labeled, stored in a cooler, and transported to the laboratory, where they were washed with alkaline water (to remove surface impurities), cut, and stored at −30°C until further processing.

Subsequently, samples were lyophilized for 24 h (Manifold Freeze Dryer MFDQ 2002, Laboquest, Westchester USA), using condenser temperature at −80°C and 1 Pa as vacuum pressure. Extraction was carried out following the method reported by Imeneo et al., with slight modifications [21]. Briefly, 2.5 g of dry CN leaves was extracted with 50 mL of absolute EtOH ($\geq$ 99.9%) two times at 40°C under magnetic stirring at 550 rpm for 60 min. Then, the solutions were centrifuged at 6000 rpm for 15 min at 4°C (Mikro 220R centrifuge, Hettich, Germany), and the supernatants were filtered under vacuum, polled, and subsequently concentrated by vacuum evaporation.

Finally, the extracts were freeze-dried, reconstituted in 1 mL of the corresponding extraction solvent to yield a final concentration of 10 mg/mL, and subjected to further analysis.

2.2 | UHPLC-HRMS/MS Conditions

UHPLC-HRMS/MS analysis was performed on a Thermo Scientific Vanquish UHPLC system coupled online to an Orbitrap Exploris 120 mass spectrometer (Thermo Fisher Scientific,

Bremen, Germany) equipped with either a heated electrospray ionization (HESI II) or an atmospheric pressure chemical ionization (APCI) source.

Chromatographic separation was carried out in the reversed-phase mode using a Kinetex 2.6 μm EVO C18 100 Å, 150 × 2.1-mm analytical column (Phenomenex, Bologna, Italy), thermostated at 40°C for HESI analysis and at 45°C for APCI analysis. Injection volume was 5 μL for both analyses.

For HESI analysis, the mobile phases consisted of H_2O (A) and ACN (B), both acidified with 0.1 (v/v %) HCOOH and delivered at a constant flow rate of 0.4 mL/min. The elution gradient was 0.01–15.00 min, 5%–20% B; 15.01–24.00 min, 20%–95% B; 24.01–30.00 min, 95%–100% B; 30.01–32.00 min, isocratic to 100% B; 32.01–34.00 min, 100%-5% B; and then 4 minutes for column re-equilibration.

For APCI analysis, the aqueous mobile phase was H_2O containing10 mM ammonium acetate (A) and the organic phase (B) was ACN/MeOH/IPA (70:20:10 v/v) (B), pumped at a constant rate of 0.4 mL/min. The elution gradient was as follows: 0.01–25.00 min, 50%–100% B; 25.01–30.00 min, isocratic to 100% B; 30.01–31.00 min, 100%-50% B, followed by 4 min re-equilibration.

Both ionization sources were operated in positive and negative mode, with calibration performed using Thermo calmix Pierce calibration solutions for both polarities.

For HESI, full MS (150–1500 m/z) and data-dependent MS/MS were acquired at 35,000 and 17,500 FWHM resolution, respectively, with NCE values of 15, 20, and 25. Source parameters were as follows: sheath gas 50 arbitrary units (a.u.), auxiliary gas 13 a.u., spray voltage +3.5/−2.8 kV, capillary temperature 310°C, and auxiliary gas heater 300°C.

For APCI, full MS (100–1500 m/z) and data-dependent MS/MS were acquired at 60,000 and 15,000 FWHM resolution, respectively, with an NCE of 30. Source parameters were as follows: sheath gas 45 a.u., auxiliary gas 5 a.u., sweep gas 1 a.u., discharge current + 4/−10 μA, capillary temperature 300°C, and auxiliary gas heater 350°C.

2.3 | Data Analysis

Data analysis and processing was performed according to a workflow previously described in our earlier study, with slight modifications [20].

FreeStyle 1.8 SP2 and Compound Discoverer 3.1 software (Thermo Scientific, SanJose, CA, U.S.A.) were employed applying a NaturalProduct Unknown ID workflow, including spectrum selection (RT 1.5–38 min, S/N = 1.5), chromatographic peak detection (mass tolerance 5 ppm, minimum intensity 1×10^4, minimum 5 scans per peak, S/N = 3, maximum peak width 1 min), and deconvolution with isotope grouping and adduct annotation. Feature alignment across samples (mass tolerance 5 ppm, RT tolerance 0.2 min) and gap filling (mass tolerance 5 ppm, S/N = 1.5) were subsequently performed to refine the dataset.

Putative metabolite identification was based on molecular formula prediction (matched), exact mass (mass tolerance < 5 ppm), and MS2 fragmentation pattern matching using Fragment Ion Search (FISh), combined with database searches against mzCloud, MassList, and ChemSpider.

To further characterize the chemical profile, data were processed using MZmine (Version 4.4.3) [22]. An untargeted LC-MS/MS workflow was applied by performing a processing mzwizard by selected UHPLC system and MS Orbitrap type. Mass detection was performed in the centroid mode within an RT range of 1.5–38 min. Chromatogram building was carried out using the ADAP algorithm (minimum four consecutive scans, minimum intensity 1×10^4, m/z tolerance 5 ppm), followed by Savitzky–Golay smoothing and feature deconvolution using the local minimum resolver (peak duration 0.05–1.5 min, minimum absolute height 2×10^4). Isotopic peak grouping (3 ppm) and feature alignment (5 ppm, RT 0.1 min) were performed using the join aligner, followed by gap filling, duplicate peak filtering, and correlation-based grouping (metaCorrelate, Pearson correlation).

Finally, spectral library searches were performed on the aligned feature list to annotate compounds by matching MS/MS spectra with MoNA (https://mona.fiehnlab.ucdavis.edu/), GNPS (https://gnps.ucsd.edu/ProteoSAFe/static/gnps-splash.jsp/), and the freely available MSnLib Mass spectral libraries (.mgf) on Zenodo (https://zenodo.org/records/11163381) [23]. All parameters for Compound Discoverer and MZmine workflows are summarized in Tables S1 and S2, respectively.

2.4 | Cell-Free In Vitro Assays

2.4.1 | Determination of TPC, Total Flavonoid Content (TFC), and Chlorophylls (CHLs), and Carotenoid (CAR) Content

CN extract was solubilized in ethanol at a final concentration of 100 μg/mL and tested for TPC and TFC determinations. TPC was assessed using a modified version of the Folin–Ciocalteu method, based on the procedure reported by Way et al. [24]. In brief, 2 μL of the extract was dispensed into a microplate well containing 100 μL of Folin–Ciocalteu reagent and mixed thoroughly. After a 5-min incubation at room temperature, 70 μL of sodium carbonate solution was added. The plate was then incubated at 40°C for 1 h. Following incubation, the absorbance was measured at 765 nm using a Multiskan Go microplate reader (Thermo Scientific, Waltham, MA, USA). A standard calibration curve was generated using gallic acid dissolved in methanol (1 mg/mL stock), with concentrations ranging from 30 to 500 μg/mL ($y = 0.0014x - 0.1549$; $R^2 = 99.62\%$). All measurements were performed in triplicate. The results were expressed as milligrams of gallic acid equivalents per gram of dry weight (mg GAE/g dw).

The TFC of the extract was quantified according to the method described by Imeneo *et al.* [21], with minor modifications. Briefly, 25 μL of sample was mixed with 100 μL of deionized water and 7.5 μL of sodium nitrite solution (5%, w/v) in a microplate well and incubated at room temperature for 5 min. Subsequently, 7.5 μL of aluminum chloride solution (10%, w/v) was added, followed by a 6-min incubation. Then, 100 μL of sodium hydroxide solution (4%, w/v) was added to complete the reaction. The mixture was allowed to react for 15 min in the dark at room temperature. Absorbance was then measured at 510 nm using a Multiskan Go microplate reader (Thermo Scientific, Waltham, MA, USA). Quantification was carried out using a standard curve prepared with rutin (30–500 μg/mL;

$y = 0.0004x - 0.0567$; $R^2 = 99.78\%$). All assays were performed in triplicate. The TFC was expressed as milligrams of rutin equivalents (RE) per gram of dry weight (mg RU/g dw).

The CHL content was determined using the methods previously described by Wang, H. *et al.* and Zhang et al., and the CAR content was determined using the method reported by Samec et al., appropriately modified [25, 26]. Briefly, 10 mg of extract was mixed with 1.25 mL of 80% acetone for 5 min on a tube mixer and then centrifuged immediately at 14,680 rpm for 10 min. The absorbance of the mixture was measured at 646.8 nm, 663.2 nm, and 452.5 nm (Multiskan SkyHigh Microplate Spectrophotometer, Thermo Fisher Scientific, Waltham, MA, USA). The chlorophyll concentration was calculated using the following formula:

$$\begin{aligned}
\text{Chl a}\,(\text{mg/gDW}) &= \frac{\{[(12.25 \times A_{663.2}) - (2.79 \times A_{646.8})] \times V\}}{m}, \\
\text{Chl b}\,(\text{mg/gDW}) &= \frac{\{[(21.50 \times A_{646.8}) - (5.10 \times A_{663.2})] \times V\}}{m}, \\
\text{Car}\,(\text{mg/gDW}) &= \frac{\{[(4.75 \times A_{452.5}) - (0.226 \times (Chla + Chlb))] \times V\}}{m}, \\
V\,&\text{extract volume}\,(\text{mL}), \\
m\,&\text{sample dry weight}\,(\text{mg}).
\end{aligned} \tag{1}$$

All analyses were carried out in triplicate, and CHL and CAR contents were expressed in micrograms per gram of dry weight (μg g^{-1} dw).

2.4.2 | 2,2-Diphenyl-1-Picrylhydrazyl (DPPH) Assay

The free radical–scavenging ability of the CN was tested using the DPPH radical-scavenging assay. The DPPH test was performed with slight modifications to the conditions reported by Noreen, H. *et al.* [27]. Briefly, 20 μL of extracts (25–100 μg/mL) or methanol as blank was mixed with 180 μL methanolic solution of DPPH (0.1 mM). All the samples were prepared in triplicate, shaken, and incubated in the dark for 30 min at 37°C. Changes in the absorbance of the samples were measured at 517 nm using a microplate reader (Multiskan Go, Thermo Scientific, Waltham, MA, USA), with methanol used as the blank. The DPPH radical-scavenging activity of the sample was expressed as Trolox equivalent antioxidant capacity (TEAC, mg TXE/g), calculated as follows: TEAC = $IC50Trolox/AIC50sample$. The higher TEAC value means a higher DPPH radical-scavenging activity.

2.4.3 | Ferric Reducing Antioxidant Power (FRAP) Assay

The assay was conducted under the conditions previously described by Aquino et al. [10]. Trolox was used as reference (1–200 μg/mL; $y = 0.0202x + 0.1323$; $R^2 = 99.99\%$). All the samples were prepared in triplicate, shaken, and incubated in the dark for 30 min at 37°C. The assay is based on the reduction of ferric-tripyridyltriazine (Fe^{3+}-TPTZ) to an intense blue color ferrous-TPTZ complex (Fe^{2+}-TPTZ). Changes in the absorbance of the samples were measured against blank at 593 nm using a microplate reader (Multiskan Go, Thermo Scientific, Waltham, MA, USA). FRAP activity was calculated as milligrams of Trolox equivalents per gram of dry weight (mg TXE g^{-1} dw).

2.5 | Cellular Assays

2.5.1 | Cell Cultures and Drug Treatment

Human hepatocellular carcinoma cell line HepG2 (HB-8065) was obtained from American Type Culture Collection (ATCC, Rockville, MD, USA). These cells were grown in the minimum essential medium (MEM, 4500 mg/mL glucose) supplemented with 10% (v/v) fetal bovine serum, 2 mM L glutamine, 100 U/mL penicillin, 0.1 mg/mL streptomycin, and 5% nonessential amino acid. Cells were routinely grown in culture dishes (Corning, Corning, NY) in an environment containing 5% CO_2 at 37°C and split every 2 days.

In each experiment, cells were placed in a fresh medium and treated with CN in the presence of a mix of OA/PA, in a 2:1 ratio, for different experimental times. As additional controls, cells were also exposed to the SIRT1 inhibitor EX527 (Sigma-Aldrich, St. Louis, MO, USA; 10 μM) and the SIRT1 activator SRT2104 (MedChemExpress, Monmouth Junction, NJ, USA; 10 μM). Each treatment and analysis were performed in at least three independent experiments carried out in triplicate.

2.5.2 | Preparation of FFA Treatments

OA and PA were purchased from Sigma-Aldrich (St. Louis, MO, USA). Stock solutions of 100 mM OA and PA were first prepared in 100% ethanol. In particular, PA was solubilized by heating at 70°C for approximately 30 min, while OA was dissolved at room temperature. To prepare the FFA–BSA conjugates, a 5% bovine serum albumin (BSA) solution was obtained by diluting a 20% BSA stock (Sigma-Aldrich) with complete MEM culture medium. OA and PA were then added to the 5% BSA solution at final concentrations of 2.5 mM and 1.25 mM, respectively, to obtain an OA/PA molar ratio of 2:1. The mixture was incubated under gentle agitation for 1 h at 37°C to allow conjugation [28–31]. For cell treatments, the conjugated FFA solution was diluted 1:5 in complete MEM medium, yielding final concentrations of 500 μM OA and 250 μM PA. A 5% BSA solution prepared under the same

conditions was used as the control and added to the cells at the same dilution as the FFA–BSA conjugates.

2.5.3 | Growth and Maturation of Spheroids in Culture

HepG2 spheroids were generated by seeding 3000 cells in 20 μL of medium as hanging drops on the inner side of 60 mm Petri dish lids. The cells aggregated by gravity at the bottom of each drop, forming a single spheroid per drop [32]. After 3 days of incubation, the spheroids were carefully collected and transferred into 24-well plates previously coated with 1% agarose to prevent cell adhesion. Once transferred, the spheroids were treated for 24 h with CN at a concentration of 50 μg/mL and a mixture of OA/PA.

2.5.4 | Cell Viability Assay

Cell viability was established by measuring mitochondrial metabolic activity with 3-(4,5-dimethylthiazol-2-yl)-2,5-diphenyl-2H-tetrazolium bromide (MTT) [33]. Briefly, HepG2 (20×10^3 cells/well) was plated into 96-well plates, and then, the CN (12.5–50 μg/mL) was added in coadministration with OA/PA for 24 h to assess cytoprotective effects in the hepatic steatotic model. Afterward, MTT reagent at 0.5 mg/mL final concentration for 2 h was added. Then, 100 μL per well of 0.1 M isopropanol/HCl solution was added to dissolve the formazan crystals. The absorbance was measured at 570 nm, using a microplate reader (Multiskan Go, Thermo Scientific, Waltham, MA, USA). Cell viability was expressed as a percentage relative to the untreated cells cultured in medium with 0.1% DMSO and set to 100%, whereas 10% DMSO was used as positive control and set to 0% of viability.

2.5.5 | Reactive Oxygen Species (ROS) Detection

ROS were quantified using 20 μM 2′,7′-dichlorodihydrofluorescein diacetate (DCFH-DA, Sigma-Aldrich) [34]. HepG2 cells (20×10^3/well) were seeded in 96-well plates and allowed to adhere for 24 h and then treated for 24 h with CN (50 μg/mL) coadministered with OA/PA. After treatment, cells were washed with PBS and incubated for 20 min at 37°C in the dark with DCFH-DA diluted in a serum-free, phenol red–free medium. The fluorescence signals (excitation/emission 485 nm/535 nm) were read in the end point mode using a PerkinElmer EnSpire multimode plate reader. The fluorescence representative images of live cells were captured using a ZOE Fluorescent Imager (Bio-Rad, Mississauga, ON, Canada) (magnification, 20x. Scale bar: 100 μm).

2.5.6 | Quantification of Cellular Glutathione (GSH) Levels

A colorimetric assay using Ellman's reagent was used for this test. The assay based on the oxidation of GSH by 5,5′-dithiobis (2-nitrobenzoic acid) (DTNB) to measure the total GSH (tGSH) content of biological samples [35]. The HepG2 cell line (1.5×10^6 cells/well) was seeded in 60-mm culture dishes and treated with CN extract (50 μg/mL) and OA/PA. After 24 h from treatments, cells were washed twice with PBS and detached with a scraper and centrifuged at655$g \times 10$ min at 4°C. Then, 100 μL of 5% (v/v) trichloroacetic acid (TCA), previously cooled to 4°C, was added to the cell pellet. Samples were incubated on ice for 15 min to promote protein precipitation. Subsequently, the samples were centrifuged at 13, 000 × g for 10 min at 4°C. The supernatant was supplemented with 1 M NaOH to neutralize the TCA for subsequent analysis with Ellman's reagent, while the pellet was used for protein quantification.

Next, in a 96-well plate, the following were added: 70 μg (in 50 μL) of total protein in reaction buffer (100 mM Na_2HPO_4 $7H_2O$, 1 mM EDTA pH 8); 30 μL (9 mM) of DTNB in reaction buffer, and 20 μL of reaction buffer. The resulting mixture was incubated for 30 min at 37°C. Absorbance was measured at 405 nm with a microplate reader (Multiskan Go, Thermo Fisher Scientific, Waltham, MA, USA). GSH (1 mM) was used as a negative control.

2.5.7 | GSH S Transferase (GST) Activity

A colorimetric assay using 1-chloro-2,4-dinitrobenzene (CDNB) was performed to measure the GST activity [36]. The HepG2 cell line was treated and lysed. The reaction mixture was first prepared: 20 μL of phosphate buffer pH 7.5; 20 μL of 1 mM reduced GSH; 20 μL of 10 mM CDNB; and 30 μL of cell lysate. After conjugation of the thiol group of GSH to the CDNB substrate, CDNB-GSH conjugation (formation of DNP-GSH conjugate by nucleophilic displacement of Cl with GSH-thiol) was measured spectrophotometrically at 340 nm. The values were expressed as the percentage of enzyme activity (U/mg protein).

2.5.8 | Lipid Peroxidation

Lipid rancidity measurements were performed using thiobarbituric acid reactive (TBAR) substances. For these analyses, a lipid peroxidation assay kit (MDA, malondialdehyde) (Sigma-Aldrich, St. Louis, MO, USA) was used for the colorimetric determination at $\lambda = 532$ nm [37]. HepG2 cells were seeded in 60-mm dishes at approximately 80% confluence. The following day, the cells were treated as previously described with 50 μg/mL of CN and OA/PA. After 24 h of incubation, the cells were detached and centrifuged at 655 × g for 10 min at 4°C. The resulting cell pellet was used to determine the MDA content in the samples, following the instructions provided with the kit.

2.5.9 | Measurement of Lactate Dehydrogenase (LDH)

HepG2 cells (20×10^3 cells/well) were seeded in 96-well plates and treated with CN (50 μg/mL) and OA/PA for 24 h. LDH release into the culture supernatant was evaluated using the LDH-Glo Cytotoxicity Assay (Promega, Wisconsin, USA) [38]. Following the manufacturer's instructions, the LDH detection reagent—containing lactate, NAD^+, reductase, reductase substrate, and Luciferase Ultra-Glo—was added to the samples. The resulting luminescent signal was quantified in endpoint mode with a PerkinElmer AlphaScreen multimode plate reader.

2.5.10 | Mitochondrial Membrane Potential Determination

Mitochondrial membrane potential was measured using tetramethylrhodamine ethyl ester (TMRE) (Invitrogen, Burlington, ON, Canada) [39]. After growing hepatocytes at 20×10^3 per well, the cells were treated with CN (50 μg/mL) and OA/PA for 24 h. The cells were then washed with PBS and incubated with 100 nM

TMRE in the serum-free medium without phenol red for 30 min at 37 °C in the dark. Excess dye was then removed by washing with PBS, and fluorescence was measured using a PerkinElmer EnSpire multimode plate reader (excitation/emission 549 nm/574 nm). The quantitative analysis is reported as the fluorescence intensity and compared to the relative controls. The fluorescence representative images of live cells were captured using a ZOE Fluorescent Imager (Bio-Rad, Mississauga, ON, Canada) (magnification, 20x. Scale bar: 100 μm).

2.5.11 | ER Expansion Evaluation

To assess the expansion of the endoplasmic reticulum (ER), a hallmark of activated ER stress, the ER-specific dye (ER-ID) Red analysis kit (Enzo Life Science, Farmingdale, NY, USA) was used to quantify ER-specific fluorescence [40]. HepG2 cells (30×10^3 cells/well) were seeded in 96-well plates and allowed to adhere for 24 h. Following this, cells were treated for 24 h with a combination of OA/PA and CN (50 μg/mL). After treatment, 100 μL of 1X assay buffer containing 1 μL of the ER-ID red detection reagent was added to each well. The plate was then incubated for 20 min at 37°C. Subsequently, cells were washed and imaged using a ZOE Fluorescent Cell Imaging System (Bio-Rad, Mississauga, ON, Canada) (magnification, 20x. Scale bar: 100 μm). ER-specific fluorescence (excitation/emission: 560 nm/630 nm) was measured using a PerkinElmer EnSpire multimode plate reader.

2.5.12 | Indirect Immunofluorescence Analysis of NF-κB Localization

HepG2 were seeded (60×10^4 cells/well) in 24-well plates containing glass cover slips, allowing them to adhere for 24 h. Then, cells were treated with CN (50 μg/mL) and OA/PA for 24h.

After treatments, cells were washed with PBS, fixed in PBS-4% paraformaldehyde, and permeabilized 10 min in PBS containing 0.25% Triton [41]. A blocking solution containing PBS-1% BSA and 50 mM NH_4Cl for 30 min was added to each well. Thereafter, cells were stained with NF-kB (Merk, Darmstadt, Germany) for 1 h.

Alexa fluor 568 antibody (Molecular Probes, Invitrogen, Waltham, Massachusetts, USA) was used as secondary antibody and incubated for 45 min. Nuclei were counterstained with 1.5 μM Hoechst 33,342 (Sigma-Aldrich, St. Louis, MO, USA) for 10 min. Images were acquired on a laser scanning confocal microscope (TCS SP8; Leica MicroSystems) equipped with a plan Apo 63X, NA 1.4 oil immersion objective lens (magnification, 63x. Scale bar: 10 μm). Quantitative analyses were performed by the ImageJ program, Version 1.47 ($N \geq 10$).

2.5.13 | Oil Red O (ORO) Staining

ORO staining was used to assess lipid droplet formation in cells. The HepG2 cells were seeded (50×10^3 cells/well) in 24-well plates and cultivated overnight. The 2D cells and spheroids [42, 43], formed as previously described, were treated with CN (50 μg/mL) and OA/PA for 24 h. The treated cells were washed twice with PBS and fixed with 10% paraformaldehyde for 15 min at room temperature, followed by 60% isopropanol incubation for 5 min. Then, the staining with ORO staining solution was performed for 20 min. Images in 2D were acquired on a fluorescence microscope (Axioshop 40, Zeiss; magnification, 20x), while the 3D images were acquired on a laser scanning confocal microscope (TCS SP8; Leica MicroSystems; magnification, 20x. Scale bar: 100 μm). Quantitative analyses were conducted by dissolving droplets in 100% isopropanol and measuring the absorbance at 510 nm [30].

2.5.14 | Real-Time PCR for Molecular Pathway Analysis

HepG2 cells were seeded in 100-mm culture dishes at 80% confluence and treated with CN (50 μg/mL) and OA/PA for 24 h. After 24 h from treatments, cells were washed twice with PBS and detached with a scraper. Total RNA was isolated using a modified procedure with the Quick-RNA Miniprep Kit (Zymo Research, CA, USA). Genomic DNA was eliminated by treatment with DNase I provided in the kit. The resulting purified RNA was then reverse transcribed into cDNA using the SensiFAST cDNA Synthesis Kit (Meridian Bioscience, EU). Real-time PCR was performed with LightCycler 480 System (La Roche Ltd.) using SYBR Green detection in a total volume of 20 μL with 1 μL of forward and reverse primers (5 μM) and 10 μL of SensiFAST SYBR No-ROX Kit (Meridian Bioscience, EU). Values were determined from the standard curve generated from serial cDNA dilutions and normalized to GAPDH.

The primers used for the real-time PCR reactions are Table 1.

The $2^{-\Delta\Delta CT}$ method was used to analyze the results, and relative mRNA expression levels were determined as fold induction relative to Ctrl cells.

2.5.15 | Flow Cytometric Analysis of SIRT1

HepG2 cells (60×10^3) were seeded into 24-well plates and incubated for 24 h with CN (50 μg/mL) and OA/PA. After treatment, the collected cells were resuspended in 50 μL FACS buffer (2% BSA, 1% formaldehyde in PBS) for 20 min. Then, cells were centrifuged at 600 g for 10 min, and the resulting pellet was resuspended in a permeabilization buffer consisting of 2% BSA, 1% formaldehyde, and 0.1% Triton X-100 in PBS [44, 45], containing the primary anti-SIRT1 antibody (*Anti-Mouse Monoclonal Antibody*, Thermo Fisher Scientific) and the Alexa Fluor 488-conjugated secondary antibody (*Anti-Mouse Secondary Antibody*, Thermo Fisher Scientific). After 30 min of incubation, the cells were centrifuged again and washed with PBS. The final pellet was resuspended in 200 μL of FACS buffer. Samples were analyzed by flow cytometry using a Becton Dickinson FACScan (Franklin Lakes, NJ, USA) equipped with CellQuest software, Version 4.

2.5.16 | SIRT1 Activity Assay

HepG2 cells were seeded in 60-mm culture dishes at a density of 1.3×10^6 cells/dish and allowed to adhere overnight. Cells were then treated with CN (50 μg/mL) and in the presence of the mixture of OA and PA. After 24 h of treatment, cells were detached and lysed according to the manufacturer's instructions using the SIRT1 Activity Assay Kit (Fluorometric, ab156065; Abcam, Cambridge, UK) [46]. The assay was performed as recommended by the supplier, and fluorescence was measured using a PerkinElmer EnSpire multimode plate reader. The results were expressed as relative SIRT1 activity, normalized to the

TABLE 1 | Forward and reverse primer sequences for target genes in real-time PCR.

	Primer sequence (5′–3′)	
Target gene	**Forward**	**Reverse**
SREBP1c	CGGAACCATCTTGGCAACA	GCCGGTTGATAGGCAGCTT
PPAR-α	AACATCCAAGAGATTTCGCAATC	CCGTAAAGCCAAAGCTTCCA
PPAR-γ	TGCAGGTGATCAAGAAGACG	AGTGCAACTGGAAGAAGGGA
FASN	TATGCTTCTTCGTGCAGCAGTT	GCTGCCACACGCTCCTCTAG
SIRT1	GCAACATCTTATGATTGGCACA	AAATACCATCCCTTGACCTGAA
FOXO1	GAGATAAGCAATCCCGAAAACA	TGGCGCAAACGAGTAGCA
NF-κB	CCCCACGAGCTTGTAGGAAAG	CCAGGTTCTGGAAACTGTGGAT
iNOS	ATGTCCGAAGCAAACATCAC	TAATGTCCAGGAAGTAGGTG
COX2	CAGCAAATCCTTGCTGTTCC	TGGGCAAAGAATGCAAACATC
GCS	CCTTCTGGCACAGCACGTTG	TAAGACGGCATCTCGCTCCT
GPx	CCTCAAGTACGTCCGACCTG	CAATGTCGTTGCGGCACACC
SOD	AGGGAACCATCCACTTCGAG	TGCGCAATCCCAATCACTCC
CAT	GCAGATACCTGTGAACTGTC	GTAGAATGTCCGCACCTGAG
BIP	CGGGCAAAGATGTCAGGAAAG	TTCTGGACGGGCTTCATAGTAGAC
IRE1α	CTCTGTCCGTACCGCCC	GAAGCGTCACTGTGCTGGT
ATF6	TTGACATTTTTGGTCTTGTGG	GCAGAAGGGGAGACACATTT

control condition obtained in the presence of the SIRT1 inhibitor EX527.

2.5.17 | Statistical Analysis

Data are reported as mean ± SD of results from three independent experiments. Statistical analysis was performed using an analysis of variance test (ANOVA), and multiple comparisons were made with the Bonferroni's test with GraphPad Prism 8.0 software (San Diego, CA, USA). Significance was assumed at $p < 0.05$.

3 | Results and Discussion

3.1 | LC-MS/MS Characterization

RP-UHPLC-Orbitrap-HRMS/MS analysis was carried out to comprehensively characterize the chemical profile of the alcoholic extract of CN leaves.

Previous LC×LC–based investigations on this species identified several major phytochemical classes, including flavonoids, phenolic acids, phenylpropanoids, isoprenoids, and saponins [20]. Those studies, however, focused on extracts prepared with an EtOH/H_2O solvent mixture [10].

In contrast, the present work employed absolute ethanol as the extraction solvent, with the purpose of obtaining a compositionally distinct extract potentially enriched in less polar constituents. This approach was designed to explore whether the different solvent polarity could influence the phytochemical composition and, consequently, the biological properties of this agri-food by-product.

To achieve a broader coverage of compounds, both $ESI^{+/-}$ and $APCI^{+/-}$ were employed. Their distinct ionization principles provided a synergistic advantage: ESI ensured the detailed characterization of more polar analytes and less polar compounds, such as glycosylated flavonoids and phenolic derivatives, as well as some CARs and chlorophyll derivatives, whereas APCI effectively captured the hydrophobic landscape, including lipids and other isoprenoid-related compounds.

As summarized in Table 2, this dual approach led to the putative identification of 53 compounds via ESI and 58 compounds using APCI, providing a more holistic view of the extract's chemical diversity.

ESI data confirmed that flavonoids represented the predominant class of compounds in the CN extract, primarily occurring as glycosides, with kaempferol and quercetin identified as the main aglycones.

This observation is consistent with previous reports on *Allium* species, where flavonoids, particularly quercetin and kaempferol derivatives, are recognized as the major phenolic constituents, especially in *Allium cepa*, in which quercetin glycosides often dominate the phytochemical profile [18, 20, 47]. Comparable trends have also been described in other species such as *A. fistulosum*, *A. porrum*, *A. sativum*, and *A. ursinum*, although differences in flavonol distribution have been reported [18, 56, 68, 69]. In this context, the flavonoid composition of the CN extract appears to be in line with the general phytochemical pattern of the genus.

Notably, ESI analysis also uncovered previously unreported CHLs and CARs, while APCI enabled a deeper characterization of lipophilic species that had been only partially resolved in earlier studies, reinforcing the necessity of a multiplatform ionization strategy for full phytochemical characterization.

CARs were predominantly detected in the ESI^+ mode. Based on their characteristic positive ion fragmentation patterns, peaks **45E** and **49E** were tentatively identified as lutein isomers,

TABLE 2 | Putatively identified compounds from the CN extract by UHPLC-Orbitrap-MS/MS analysis.

Peak*	Rt (min)	Compounds	m/z	MS2	Chemical formula	Error (ppm)	Reference ion	Class	References
Electrospray ionization (ESI)									
1E	8.48	Quercetin 3-sophorotrioside	787.1949	300.0281; 271.0256; 255.0309; 151.0029	$C_{33}H_{40}O_{22}$	−4.96	$[M-H]^-$	Flavonoids	[47]
2E	9.05	Ferulic acid	193.0501	178.0264; 149.0599; 134.0363	$C_{10}H_{10}O_4$	1.95	$[M-H]^-$	Phenylpropanoids	[48]
3E	10.62	Kaempferol 3,7-*O*-diglucoside (Allivicin)	609.1466	489.1031; 401.1822; 285.0405; 175.1357	$C_{27}H_{30}O_{16}$	2.42	$[M-H]^-$	Flavonoids	[48–50]
4E	10.52	Quercetin 3,4′-di-*O*-beta-D-glucopyranoside	625.1412	463.0887; 301.0355	$C_{27}H_{30}O_{17}$	2.58	$[M-H]^-$	Flavonoids	[47, 50]
5E	10.57	Quercetin 3-*O*-glucoside	465.1035	303.0503	$C_{21}H_{20}O_{12}$	1.71	$[M+H]^+$	Flavonoids	[51]
6E	10.68	6-Hydroxyluteolin 7-*O*-rhamnoside (*isomer I*)	449.1084	287.0555; 329.0522	$C_{21}H_{20}O_{11}$	3.29	$[M+H]^+$	Flavonoids	[48]
7E	10.7	Cyanidin 3,5-*O*-diglucoside	611.1616	449.1082; 287.0552; 145.0495; 85.029	$C_{27}H_{31}O_{16}$	0.66	$[M+H]^+$	Flavonoids	[48]
8E	12.08	Kaempferol 3,7-*O*-diglucoside	609.1463	485.2004; 285.0405; 151.0029; 178.998	$C_{27}H_{30}O_{16}$	2.42	$[M-H]^-$	Flavonoids	[48, 49]
9E	12.77	Quercetin 3,4′-di-*O*-beta-D-glucopyranoside	625.1417	463.089; 301.0354	$C_{27}H_{30}O_{17}$	2.49	$[M-H]^-$	Flavonoids	[47, 50]
10E	12.91	Quercetin-3-*O*-*β*D-glucopyranoside (isoquercetin)	463.0884	301.0352; 178.9974; 151.0024	$C_{21}H_{20}O_{12}$	2.69	$[M-H]^-$	Flavonoids	[48]
11E	14.82	Kaempferol hexoside (*isomer I*)	447.0936	327.0511; 284.0328; 447.1080; 255.0312	$C_{21}H_{20}O_{11}$	2.81	$[M-H]^-$	Flavonoids	[49]
12E	15.25	Kaempferol hexoside (*isomer II*)	447.0937	327.0508; 285.0406; 255.0308; 284.0327; 447.0936	$C_{21}H_{20}O_{11}$	2.95	$[M-H]^-$	Flavonoids	[49]
13E	14.87	Quercetin-3-*O*-*β*D-glucopyranoside (isoquercetin)	463.0886	301.0354; 178.9983; 151.0025	$C_{21}H_{20}O_{12}$	3.42	$[M-H]^-$	Flavonoids	[48]
14E	14.89	Quercetin (*isomer I*)	301.0349	178.9979; 151.0027	$C_{15}H_{10}O_7$	3.93	$[M-H]^-$	Flavonoids	[48]
15E	14.92	Quercetin 3-*O*-glucoside	465.103	303.0502	$C_{21}H_{20}O_{12}$	0.85	$[M+H]^+$	Flavonoids	[51]
16E	14.95	6-Hydroxyluteolin 7-*O*-rhamnoside (*isomer II*)	449.1079	287.0554	$C_{21}H_{20}O_{11}$	1.79	$[M+H]^+$	Flavonoids	[48]
17E	15.39	Isorhamnetin hexoside (*isomer I*)	477.1045	357.0596; 314.0435; 178.9977; 151.0026	$C_{22}H_{22}O_{12}$	2.81	$[M-H]^-$	Flavonoids	[49]

(Continues)

TABLE 2 | (Continued)

Peak*	Rt (min)	Compounds	m/z	MS2	Chemical formula	Error (ppm)	Reference ion	Class	References
18E	16.44	Isorhamnetin hexoside (*isomer II*)	477.1045	357.0612; 314.0435; 153.0191	$C_{22}H_{22}O_{12}$	2.43	$[M-H]^-$	Flavonoids	[49]
19E	15.53	Quercetin 3-[2‴-(*E*)-caffeoyl sophoroside]-7-glucoside	963.2431	787.1949; 301.035; 178.998	$C_{43}H_{48}O_{25}$	2.93	$[M-H]^-$	Flavonoids	[49, 52]
20E	16.11	Quercetin-3-*O*-feruloyl-sophoroside-7-*O*-D-glucoside	963.2433	787.1962; 301.035; 178.9981	$C_{43}H_{48}O_{25}$	2.43	$[M-H]^-$	Flavonoids	[49, 52]
21E	16.15	Kaempferol-3-*O*-coumaroyldiglucoside-7-*O*-glucoside	917.2375	771.1992; 591.139; 285.0405	$C_{42}H_{46}O_{23}$	2.2	$[M-H]^-$	Flavonoids	[49, 52]
22E	16.57	Kaempferol-3-*O*-feruloyldiglucoside-7-*O*-glucoside (*isomer I*)	947.2477	771.201; 609.1489; 489.1191; 285.0405	$C_{43}H_{48}O_{24}$	3.09	$[M-H]^-$	Flavonoids	[49, 52]
23E	17.79	Kaempferol-3-*O*-feruloyldiglucoside-7-*O*-glucoside (*isomer II*)	947.2484	771.1993; 285.0411	$C_{43}H_{48}O_{24}$	2.45	$[M-H]^-$	Flavonoids	[49, 52]
24E	17.81	Neohecogenin-3-O*β*-D-glucopyranosyl (1→2)-*β*-D-glucopyranosyl (1→4)-*β*-D-galactopyranoside	901.4795	269.1900; 287.2009; 413.3049; 595.3123	$C_{45}H_{72}O_{18}$	0.32	$[M+H]^+$	Steroidal glycosides	[10, 20]
25E	18.06	Pennogenin-3-*O*-*α*-L-arabinofuranosyl(1→4)[*α*-L-rhamnopyranosyl(1→2)]-*β*-D-glucopyranoside	871.4682	709.4157; 413.3049; 269.1901; 287.2009	$C_{44}H_{70}O_{17}$	1.88	$[M+H]^+$	Steroidal glycosides	[10, 20]
26E	18.12	Quercetin (*isomer II*)	301.0353	178.9978; 151.0027	$C_{15}H_{10}O_7$	3.52	$[M-H]^-$	Flavonoids	[50]
27E	18.94	Kaempferol 3-*O*-feruloylsophoroside	785.1951	285.0403; 284.0327; 609.1461	$C_{33}H_{38}O_{22}$	18.92	$[M-H]^-$	Flavonoids	[50, 53]
28E	19.4	Palmitoylglycine (*isomer I*)	314.2693	240.2319; 296.2588; 60.0443; 90.0548; 72.0443	$C_{18}H_{35}O_3N$	−0.06	$[M+H]^+$	Lipids	[20]
29E	19.45	Isorhamnetin	317.066	285.0496; 151.0038	$C_{16}H_{12}O_7$	0.68	$[M+H]^+$	Flavonoids	[48]
30E	19.65	Dehydrophytosphingosine	316.2846	298.2747; 280.2637; 262.2536; 60.0443; 250.2529	$C_{18}H_{37}O_3N$	0.44	$[M+H]^+$	Lipids	[20]
31E	19.79	*α*-Linolenic acid	279.2326	261.2217; 247.0990; 95.0859	$C_{18}H_{30}O_2$	0.82	$[M+H]^+$	Lipids	[20]
32E	19.81	Palmitoylglycine (*isomer II*)	314.2693	296.2588; 279.2321; 72.045	$C_{18}H_{35}O_3N$	0.33	$[M+H]^+$	Lipids	[20]
34E	20.12	Phytosphingosine	318.3004	60.0451; 300.2899; 282.2794	$C_{18}H_{39}O_3N$	0.45	$[M+H]^+$	Lipids	[10]

(Continues)

TABLE 2 | (Continued)

Peak*	Rt (min)	Compounds	m/z	MS2	Chemical formula	Error (ppm)	Reference ion	Class	References
35E	20.67	N-Acetylsphinganine	344.3159	300.2899; 282.2792; 326.3059; 88.0761; 60.0451	$C_{20}H_{41}O_3N$	−0.19	$[M+H]^+$	Lipids	[54]
36E	22.02	LPC 18:2	520.3395	184.0735; 104.1074	$C_{26}H_{50}O_7NP$	0.5	$[M+H]^+$	Lipids	[54]
37E	22.36	LPC 16:0	496.3401	184.0736; 104.1074; 478.3296	$C_{24}H_{50}O_7NP$	0.34	$[M+H]^+$	Lipids	[10]
38E	22.77	α-Linolenoyl ethanolamide	322.2743	62.0607; 234.9611; 305.2466	$C_{20}H_{35}O_2N$	−0.5	$[M+H]^+$	Lipids	[10]
39E	23.4	Linoleoyl ethanolamide	324.2899	62.0607; 307.2635; 263.2375; 245.2273; 179.1798	$C_{20}H_{37}O_2N$	0.46	$[M+H]^+$	Lipids	[10]
40E	23.93	α-Linolenic acid	279.2322	95.086; 109.1015; 81.0705; 123.117	$C_{18}H_{30}O_2$	1.37	$[M+H]^+$	Lipids	[55]
41E	24.42	Oleamide	282.2794	247.2423; 265.2524; 97.1017	$C_{18}H_{35}ON$	1.09	$[M+H]^+$	Lipids	[20]
42E	24.92	Pheophorbide a (*isomer I*)	593.2764	533.2548; 565.2811	$C_{35}H_{36}O_5N_4$	0.47	$[M+H]^+$	Chlorophylls	[56, 57]
43E	25.76	DG 36:6	613.4821	595.473; 335.2584	$C_{39}H_{64}O_5$	1.12	$[M+H]^+$	Lipids	[10]
44E	26.08	Echinenone	551.425	175.144; 119.0858; 145.1015	$C_{40}H_{54}O$	0.89	$[M+H]^+$	Carotenoids	[58]
45E	27.36	Lutein (*isomer I*)	569.4351	551.4253	$C_{40}H_{56}O_2$	2.03	$[M+H]^+$	Carotenoids	[59]
46E	29.08	Pheophytin a (*isomer I*)	871.5738	539.2766; 533.2552	$C_{55}H_{74}O_5N_4$	0.96	$[M+H]^+$	Chlorophylls	[56, 57]
47E	30.11	Hydroxypheophytin a (*isomer I*)	887.5682	609.2692; 549.2486	$C_{55}H_{74}O_6N_4$	−0.07	$[M+H]^+$	Chlorophylls	[60]
48E	31.37	Pheophytin b	885.552	607.2556; 547.2344	$C_{55}H_{72}O_6N_4$	0.51	$[M+H]^+$	Chlorophylls	[56, 57, 60]
49E	31.47	Lutein (*isomer II*)	569.4350	551.4255	$C_{40}H_{56}O_2$	−1.29	$[M+H]^+$	Carotenoids	[56]
50E	32.06	15^1-Hydroxy-lactone-pheophytin a	903.5627	625.2659	$C_{55}H_{74}O_7N_4$	0.29	$[M+H]^+$	Chlorophylls	[57]
51E	32.22	Hydroxypheophytin a (*isomer II*)	887.5682	609.2717; 591.2609; 549.2483	$C_{55}H_{74}O_6N_4$	0.07	$[M+H]^+$	Chlorophylls	[60]
52E	32.97	Pheophytin a (*isomer II*)	871.5704	593.2761; 533.2553	$C_{55}H_{74}O_5N_4$	−0.79	$[M+H]^+$	Chlorophylls	[57]
53E	33.38	Pheophorbide a (*isomer II*)	593.2759	533.2514; 565.2777; 251.3165	$C_{35}H_{36}O_5N_4$	0.98	$[M+H]^+$	Chlorophylls	[57]

(Continues)

TABLE 2 | (Continued)

Peak*	Rt (min)	Compounds	m/z	MS2	Chemical formula	Error (ppm)	Reference ion	Class	References
Atmospheric pressure chemical ionization (APCI)									
1A	0.67	Alliin	178.0529	88.0392; 42.0338; 91.0212; 114.0371	$C_6H_{11}NO_3S$	−2.16	$[M+H]^+$	Amino acids, peptides, and analogs	[20]
2A	6.40	Monolinolenin (2-linolenoylglycerol)	353.2678	335.2592; 261.2210; 243.2102; 279.2318	$C_{21}H_{36}O_4$	0.28	$[M+H]^+$	Lipids	[22]
3A	6.61	MGMG 18:3	532.3467	353.2686; 335.2573; 261.2209; 243.2104	$C_{27}H_{46}O_9$	0.13	$[M+NH_4]^+$	Lipids	[22]
4A	7.26	α-Linolenic acid	277.2170	59.0140; 233.2271; 259.2068	$C_{18}H_{30}O_2$	−1.16	$[M-H]^-$	Lipids	[55]
5A	8.08	α-Linolenoyl ethanolamide	322.2733	62.0599; 261.2207; 304.2634	$C_{20}H_{35}NO_2$	0.39	$[M+H]^+$	Lipids	[22]
6A	9.27	Linoleic acid	279.2325	261.2229; 71.4639; 112.0822; 149.8636; 194.0919	$C_{18}H_{32}O_2$	−1.24	$[M-H]^-$	Lipids	[22]
7A	9.97	Linoleoyl ethanolamide	324.2890	62.0599; 245.2264; 263.2369; 306.2789	$C_{20}H_{37}NO_2$	0.45	$[M+H]^+$	Lipids	[22]
8A	10.64	Palmitic acid	255.2325	237.8235; 97.6534; 138.4916; 147.5438; 199.9075	$C_{16}H_{32}O_2$	−1.66	$[M-H]^-$	Lipids	[61]
9A	11.25	Palmitoyl ethanolamide	300.289	283.2620; 239.2364; 62.0599	$C_{18}H_{37}NO_2$	−1.04	$[M+H]^+$	Lipids	[22]
10A	11.85	N-Acetylsphinganine	344.3150	60.0443; 88.0755; 300.2894; 282.2787	$C_{20}H_{41}NO_3$	−2.76	$[M+H]^+$	Lipids	[22]
11A	12.18	N-Oleoylethanolamine	326.3047	309.2779; 247.2418; 62.0599; 265.2531	$C_{20}H_{39}NO_2$	−0.71	$[M+H]^+$	Lipids	[22]
12A	14.52	Stearic acid	283.2639	265.2500; 177.7347; 194.8538; 239.2507; 258.1577	$C_{18}H_{36}O_2$	−1.19	$[M-H]^-$	Lipids	[18, 31]

(Continues)

TABLE 2 | (Continued)

Peak*	Rt (min)	Compounds	m/z	MS2	Chemical formula	Error (ppm)	Reference ion	Class	References
13A	16.13	FA 24:0; O	383.3525	337.3477; 69.0347; 83.0502; 106.0661; 113.0248; 186.0627; 195.3139	$C_{24}H_{48}O_3$	−1.54	$[M-H]^-$	Lipids	[54]
14A	17.94	ST 29:2; O;Hex	633.4367	89.0244; 71.0138; 101.0245; 119.0350; 113.0245; 179.0560; 573.4161	$C_{35}H_{58}O_6$	0.59	$[M-H+HAc]^-$	Lipids	[54]
15A	18.20	PE 34:4	712.4895	571.4891; 597.4867; 81.0699; 95.0854; 261.2208; 335.2566;	$C_{39}H_{70}NO_8P$	−2.36	$[M+H]^+$	Lipids	[62]
16A	18.31	PE 36:5	738.5049	597.4874; 548.4667; 417.2924; 263.2385; 337.2721	$C_{41}H_{72}NO_8P$	−1.23	$[M+H]^+$	Lipids	[22]
17A	19.01	PA 36:4	695.4656	279.2329; 152.9959; 78.9591; 415.2254; 96.9696	$C_{39}H_{69}O_8P$	1.36	$[M-H]^-$	Lipids	[54]
18A	19.05	Zeaxanthin	569.4339	551.4288; 534.4861; 431.3326	$C_{40}H_{56}O_2$	−0.64	$[M+H]^+$	Carotenoids	[22, 59]
19A	19.10	PE 34:3	714.5046	599.5027; 573.4865; 263.2366; 81.0697; 109.1010; 337.2740; 155.0099	$C_{39}H_{72}NO_8P$	1.36	$[M+H]^+$	Lipids	[54]
20A	19.69	DGDG 36:6	954.6124	335.2578; 261.2213; 595.4689	$C_{51}H_{88}NO_{15}$	−2.54	$[M+NH_4]^+$	Lipids	[63]
21A	19.70	Di-γ-linolenin	613.4816	595.4727; 521.4341; 261.2213; 335.2577	$C_{39}H_{64}O_5$	1.28	$[M+H]^+$	Lipids	[22]
22A	19.75	Ginsenoside Rh2	621.4371	308.3076; 134.0761; 390.3336; 530.3862; 170.5041; 98.9521	$C_{36}H_{62}O_8$	−0.19	$[M-H]^-$	Terpene glycosides	[22]
23A	19.91	PE 34:2 (*isomer I*)	716.5208	575.5030; 263.2367; 239.2368;	$C_{39}H_{74}NO_8P$	0.59	$[M+H]^+$	Lipids	[54]

(Continues)

TABLE 2 | (Continued)

Peak*	Rt (min)	Compounds	m/z	MS2	Chemical formula	Error (ppm)	Reference ion	Class	References
24A	20.13	PE 36:6	736.4896	595.4716; 696.2568; 500.4456; 261.2222; 335.2562	$C_{41}H_{70}NO_8P$	−1.03	$[M+H]^+$	Lipids	[22]
25A	20.78	FA 22:0	339.3265	61.6178; 106.9795; 114.4943; 138.9756; 145.4787; 182.5089; 191.7177; 192.5654; 228.9366	$C_{22}H_{44}O_2$	−1.38	$[M-H]^-$	Lipids	[54]
26A	21.21	MGDG 36:6	792.5597	595.4697; 335.2580; 261.2213; 95.0855; 121.1011; 173.1325; 317.2475	$C_{45}H_{74}O_{10}$	−3.25	$[M+NH_4]^+$	Lipids	[54]
27A	21.70	DGDG 34:3 (*isomer I*)	959.5943	277.2173; 255.2328; 397.1349; 415.1453; 101.0244; 913.5890	$C_{49}H_{86}O_{15}$	0.69	$[M-H+HAc]^-$	Lipids	[64]
28A	21.76	DGDG 34:3 (*isomer II*)	932.6279	313.2737; 335.2579; 261.2211; 573.4869; 109.1014; 145.0496	$C_{49}H_{86}O_{15}$	−2.75	$[M+NH_4]^+$	Lipids	[63]
29A	22.01	FA 23:0	353.3422	52.0230; 66,3141; 146.7255; 164.4188; 224.1623; 254.9975; 271.2473	$C_{23}H_{46}O_2$	−0.87	$[M-H]^-$	Lipids	[62]
30A	22.21	MGDG 36:5	794.5753	337.2738; 597.4882; 261.2213; 109.1012; 95.0854	$C_{45}H_{76}O_{10}$	1.71	$[M+NH_4]^+$	Lipids	[54]
31A	22.34	PE 36:4 (*isomer I*)	738.5079	279.2329; 280.2364; 140.0118; 476.2786; 196.0379	$C_{41}H_{74}NO_8P$	1.16	$[M-H]^-$	Lipids	[54]
32A	22.36	PE 36:4 (*isomer II*)	740.5206	599.5027; 81.0698; 109.1011; 263.2365	$C_{41}H_{74}NO_8P$	−2.44	$[M+H]^+$	Lipids	[63]
34A	22.55	PE 33:2	702.5057	561.4868; 263.2357; 337.2741; 225.2211	$C_{38}H_{72}NO_8P$	−0.26	$[M+H]^+$	Lipids	[22]

(Continues)

TABLE 2 | (Continued)

Peak*	Rt (min)	Compounds	m/z	MS2	Chemical formula	Error (ppm)	Reference ion	Class	References
35A	22.69	DGDG 34:2 (*isomer I*)	961.6101	279.2328; 255.2328; 397.1349; 415.1454; 101.0244;	$C_{49}H_{88}O_{15}$	0.76	$[M-H+HAc]^-$	Lipids	[64]
36A	22.74	DGDG 34:2 (*isomer II*)	934.6438	313.2736; 337.2736; 575.5029; 239.2376	$C_{49}H_{88}O_{15}$	−2.58	$[M+NH_4]^+$	Lipids	[63]
37A	22.88	Stigmasterol	395.3667	81.0700; 159.1177; 95.0854; 109.1014; 177.1645; 255.2109	$C_{29}H_{48}O$	−0.33	$[M+H-H_2O]^+$	Steroids	[65]
38A	23.06	FA 24:0; O	367.3575	51.2549; 63.2523; 228.9508; 266.9189	$C_{24}H_{48}O_2$	−1.31	$[M-H]^-$	Lipids	[17]
39A	23.13	MGDG 36:4	796.5910	337.2736; 599.5026; 617.5150; 95.0854; 263.2373	$C_{45}H_{78}O_{10}$	0.53	$[M+NH_4]^+$	Lipids	[63]
40A	23.22	Monoelaidin	339.2895	308.8995; 265.2529; 214.1314; 279.6796; 69.0698; 83.0854; 95.0853	$C_{21}H_{40}O_4$	1.28	$[M+H-H_2O]^+$	Lipids	[22]
41A	23.32	PE 34:2 (*isomer I*)	714.5079	279.2328; 255.2328; 140.0119; 196.0379; 452.2777	$C_{39}H_{74}NO_8P$	−0.08	$[M-H]^-$	Lipids	[64]
42A	23.38	PE 34:2 (*isomer II*)	716.5206	575.5026; 95.0854; 239.2367; 81.0697; 109.1011	$C_{39}H_{74}NO_8P$	−2.50	$[M+H]^+$	Lipids	[63]
43A	23.42	PE 36:3	742.5361	601.5184; 575.5033; 265.2530; 337.2748	$C_{41}H_{66}NO_8P$	−1.44	$[M+H]^+$	Lipids	[22]
44A	24.13	DG (36:5)	632.5237	337.2732; 261.2210; 597.4878; 469.3490	$C_{39}H_{66}O_5$	−0.82	$[M+NH_4]^+$	Lipids	[22]
45A	24.18	Ornithine lipid derivative	665.5812	115.0865; 351.3004; 552.3362; 369.3107	$C_{40}H_{76}N_2O_5$	1.02	$[M+H]^+$	Lipids	[66]
46A	24.80	Monopalmitolein	311.2577	275.2000; 241.0395; 225.0433	$C_{19}H_{36}O_4$	1.9	$[M+H-H_2O]^+$	Lipids	[22]
47A	24.91	FA 26:0	395.3891	61.1764; 134.4456; 228.9383	$C_{26}H_{52}O_2$	2.57	$[M-H]^-$	Lipids	[62]
48A	24.93	DG 36:4	634.5393	599.5026; 337.2734; 263.2372	$C_{39}H_{68}O_5$	−0.24	$[M+NH_4]^+$	Lipids	[22]

(Continues)

TABLE 2 | (Continued)

Peak*	Rt (min)	Compounds	m/z	MS2	Chemical formula	Error (ppm)	Reference ion	Class	References
49A	25.44	α-Tocopherol (Vitamin *E*)	430.3783	165.0908; 360.0287; 289.2167; 205.1223	$C_{29}H_{50}O_2$	−0.05	$[M+H]^+$	Tocopherols	[22]
50A	25.72	Chlorophyll a	893.5409	615.2418; 555.2231, 614.2365; 833.5206	$C_{55}H_{72}N_4O_5Mg$	−1.58	$[M+H]^+$	Chlorophylls	[22, 57, 59]
51A	25.99	β-Cryptoxanthin	553.4403	535.4289; 335.2736; 497.2682	$C_{40}H_{56}O$	−0.78	$[M+H]^+$	Carotenoids	[22]
52A	26.50	1-Palmitoyl-2-oleoyl-sn-glycerol	577.5186	418.9932; 355.0693; 265.2528	$C_{37}H_{70}O_5$	1.72	$[M+H-H_2O]^+$	Lipids	[22]
53A	26.65	DG 36:6	613.4815	595.4726; 335.2584; 261.2209; 109.1011	$C_{39}H_{64}O_5$	−1.97	$[M+H]^+$	Lipids	[54]
54A	26.66	Monoolein (2-oleoylglycerol)	339.2889	83.0854; 95.0854; 135.1167; 149.1323; 247.2415; 265.2518; 322.2477	$C_{21}H_{40}O_4$	−2.01	$[M+H-H_2O]^+$	Lipids	[22]
55A	27.56	Cer 42:1; O3	682.6332	280.2632; 262.2527; 298.2737; 316.3838; 646.6121; 133.1010; 384.3831	$C_{42}H_{83}NO_5$	−1.66	$[M+H]^+$	Lipids	[54]
56A	28.32	Pyropheophytin a	813.5657	535.2694; 461.2354	$C_{53}H_{72}N_4O_3$	−0.49	$[M+H]^+$	Chlorophylls	[22, 59]
57A	28.35	Pheophytin a (*isomer I*)	870.5649	515.2452; 559.2347; 461.2338; 315.9254	$C_{55}H_{74}N_4O_5$	−0.57	$[M-H]^-$	Chlorophylls	[54]
58A	28.73	Pheophytin a (*isomer II*)	871.5714	539.2766; 533.2552	$C_{55}H_{74}N_4O_5$	0.28	$[M]^+$	Chlorophylls	[58, 67]

*E = Electrospray ionization (ESI); A = atmospheric pressure chemical ionization (APCI).

showing a precursor ion $[M+H]^+$ at *m/z* 569 and diagnostic product ions at *m/z* 551 (loss of H_2O) [59].

These compounds are well-known constituents of photosynthetic tissues and have been previously reported in several *Allium* species, including *A. fistulosum*, where lutein and zeaxanthin represent the major CARs [70].

In addition to CARs, ESI^+ analysis revealed the presence of multiple chlorophyll derivatives, suggesting the occurrence of chlorophyll degradation processes within the plant matrix, including pheophytin a (peaks **46E** and **52E**, *m/z* 871), pheophytin *b* (peak **48E**, *m/z* 885), hydroxypheophytin a (peaks **47E** and **51E**, *m/z* 887), and pheophorbide a (peaks **42E** and **53E**, *m/z* 593). Similar compounds have been previously identified in *A. ursinum* leaves, supporting their role as common chlorophyll catabolites in the genus [56].

The observed fragmentation pathways, mainly involving the loss of the phytyl chain (as the phytadiene, $C_{20}H_{38}$, $[M+H-278]^+$) and subsequent cleavage reactions ($[M+H - C_{20}H_{38} - COOCH_3]^+$), agree with those reported for chlorophyll derivatives in plant matrices (Figure 1) [57].

The APCI approach provides a more in-depth characterization of the pigments and lipidic components in the CN extract.

Complementing ESI data, APCI facilitated the detection of CARs including zeaxanthin (compound **18A**, $[M+H]^+$, *m/z* 569) and *β*-cryptoxanthin (compound **51A**, $[M+H]^+$, *m/z* 553). Both compounds exhibited a predominant fragment ion due to dehydration, at m/z 551 and m/z 535, respectively, similar to the fragmentation behavior of lutein.

Unlike zeaxanthin, whose presence is consistent with previous findings in *Allium* species, the detection of *β*-cryptoxanthin is less commonly reported in this genus, suggesting possible species-specific variability or differences related to the analyzed matrix [70].

Additionally, several lipid subclasses were tentatively identified, including FAs, digalactosyldiacylglycerols (DGDGs), monogalactosyldiacylglycerols (MGDGs), phosphatidylethanolamines (PEs), and phosphatidic acids (PAs). The compounds were mainly detected as $[M-H]^-$ and $[M+H]^+$ ions, but also as adducts such as $[M-H+HAc]^-$ and $[M+NH_4]^+$, in agreement with their expected ionization behavior and consistent with previously reported data [71].

MGDG 36:4 (compound **39A**, $C_{45}H_{76}O_{10}$) was detected as the $[M+NH_4]^+$ adduct at *m/z* 796. The subclass was tentatively assigned based on the observed neutral loss of $C_6H_{11}O_6$ (179 Da), corresponding to the galactosyl moiety as well as the loss of the ammonium adduct (18 Da), which generated a fragment ion at *m/z* 599 ($C_{39}H_{67}O_4^+$). Additionally, the fragmentation pattern suggested the presence of an 18:2 fatty acyl chain, indicated by the diagnostic ion at *m/z* 337 ($C_{21}H_{37}O_3^+$) (Figure 2). Similarly, MGDG 36:5 (compound **30A**, $C_{45}H_{76}O_{10}$) was detected as the $[M+NH_4]^+$ adduct at *m/z* 794 with main fragment ion at *m/z* 597, and MGDG 36:6 (compound **26A**, $C_{45}H_{74}O_{10}$) was detected as the $[M+NH_4]^+$ adduct at *m/z* 792 with main fragment ion at *m/z* 595.

APCI analysis allowed the detection of FAs in CN extracts. In particular, medium-chain FAs (MFAs) such as linolenic acid, linoleic acid, PA, and stearic acid were identified. These compounds were detected as deprotonated molecular ions $[M-H]^-$, exhibiting characteristic fragment ions corresponding to $[M-H-18]^-$, $[M-H-44]^-$, and $[M-H-18-44]^-$, indicative of neutral losses of H_2O and CO_2 molecules.

For instance, compound **4A** was identified as linolenic acid, showing a precursor ion at *m/z* 277. The fragmentation pattern included ions at *m/z* 259 and 233, corresponding to the neutral loss of H_2O (18 Da) and CO_2 (44 Da), respectively (Figure 3). A similar fragmentation behavior was observed for linoleic acid (precursor ion at *m/z* 279), which produced a main fragment ion at m/z 261, corresponding to the $[M-H-18]^-$ species [61].

Overall, the lipidomic profile obtained in this study highlights the occurrence of several lipid subclasses, including FAs, glycolipids (MGDGs and DGDGs), and phospholipids such as PE and PA. Rather than representing isolated findings, this distribution is consistent with the general lipid composition previously described for *Allium* spp., where membrane-associated lipids constitute a major fraction of the total lipidome [72]. Their presence in the analyzed samples is therefore in agreement with previous lipidomic investigations on *Allium* spp., reinforcing the reliability of the tentative assignments and indicating a conserved lipid signature within the genus. Indeed, the presence of unsaturated FAs, particularly linolenic, linoleic, palmitic, and stearic acids, is not unexpected, as they are widely recognized as characteristic components of *Allium* lipid profiles and contribute to both membrane fluidity and important physiological and signaling processes in plants [72, 73].

3.2 | Evaluation of Polyphenol and Flavonoid Content and In Vitro Antioxidant Effect of CN Extract

The extract was first analyzed using the Folin–Ciocalteu method to estimate its TPC, and the aluminum chloride method was employed to evaluate flavonoid levels, both tested at a final concentration of 100 μg/mL.

The TPC was calculated from the regression equation of the gallic acid calibration curve and expressed as gallic acid equivalents (GAEs), giving a value of 78.04 ± 0.03 mg GAE/g for the CN extract.

Similarly, the TFC was obtained from the regression equation of the rutin calibration curve and reported in REs, resulting in a concentration of 59.36 ± 0.02 mg RE/g for the CN extract.

Figure S1 illustrates the results of the spectrophotometric analysis: CHL content was $380.92 \pm 10.08\ \mu g\ g^{-1}$ dw, with chlorophyll a (Chl a) and chlorophyll b (Chl b) contributing 252.24 ± 6.93 and $128.68 \pm 3.77\ \mu g\ g^{-1}$ dw, respectively. The total CAR content was $151.41 \pm 4.38\ \mu g\ g^{-1}$ dw. Compared to reference values reported in the literature (CHLs: $156.05 \pm 9.26\ \mu g\ g^{-1}$ dw; Chl a: $79.73 \pm 5.94\ \mu g\ g^{-1}$ dw; Chl b: $54.16 \pm 2.19\ \mu g\ g^{-1}$ dw), the CN extract exhibited significantly higher pigment concentrations [69]. Comparable values were reported for particularly pigment-rich specimens [74].

The antioxidant capacity of the CN extract was evaluated through DPPH and FRAP assays.

Regarding DPPH assay, the results were expressed as TEAC (mg TXE/g), based on a Trolox calibration curve within the range of

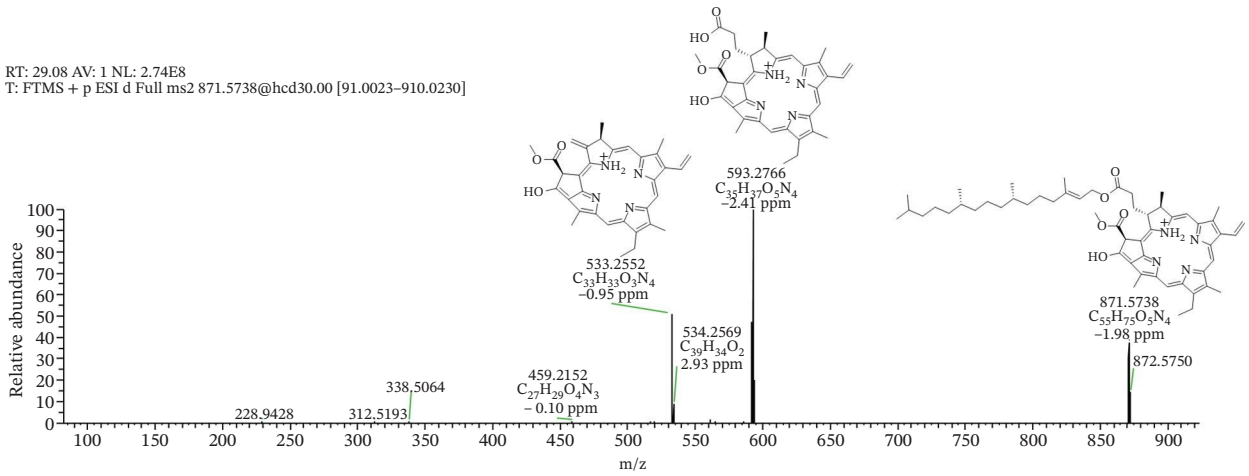

FIGURE 1 | Representative ESI + fragmentation pattern of pheophytin a.

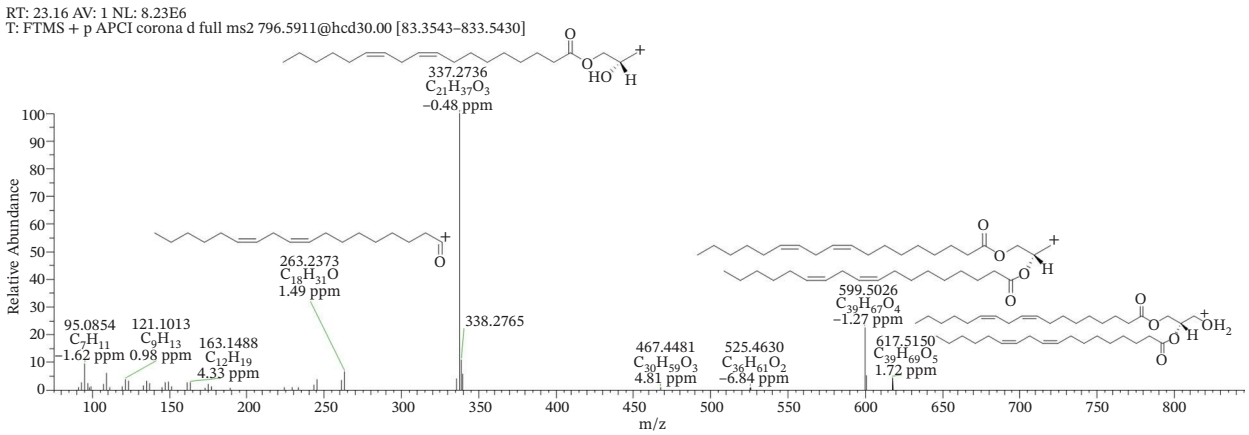

FIGURE 2 | Representative APCI $^{+}$ fragmentation pattern of monogalactosyldiacylglycerols (MGDGs) 36:4.

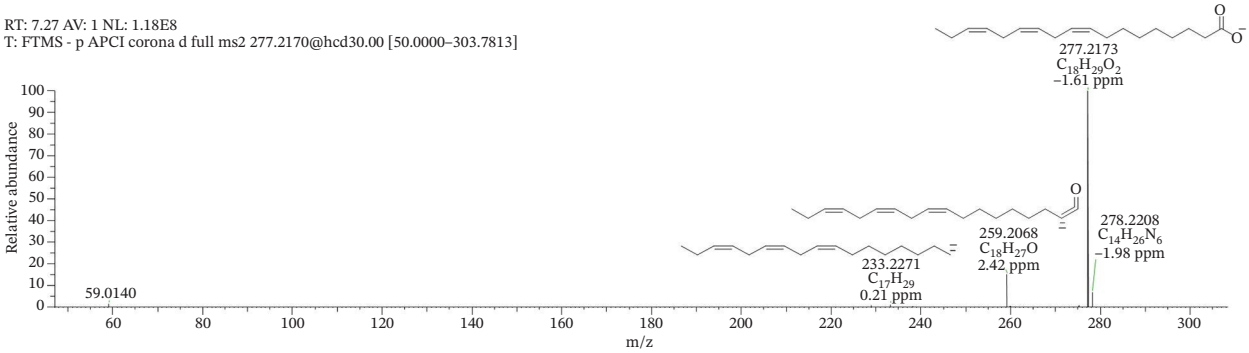

FIGURE 3 | Representative APCI^{-} fragmentation pattern of α-linolenic acid.

0.025–0.2 mg. The extract was tested at concentrations between 25 and 100 μg/mL, and radical-scavenging activity was determined using the equations described in the experimental section. The data revealed a concentration-dependent increase in radical-scavenging activity in the DPPH assay, with a TEAC value of 153.86 ± 1.07 mg TXE/g for CN, indicating a strong antioxidant effect of the extract when compared to Trolox, employed as the reference standard.

The FRAP assay was also carried out to support these findings. This method relies on the reduction of Fe^{3+} to Fe^{2+} by antioxidants in the presence of TPTZ, generating a blue Fe^{2+}–TPTZ complex. The CN extract, tested at 25–100 μg/mL, showed a scavenging capacity equivalent to 6.49 ± 0.04 mg TXE g^{-1} dw at 100 μg/mL.

3.3 | Cellular Investigation

3.3.1 | Antisteatotic Effects of CN Extract

First, the MTT cell viability assay was conducted to evaluate the potential cytotoxic effects of different concentrations of the CN extract. HepG2 cells were exposed to increasing concentrations of CN extract ranging between 50 and 12.5 μg/mL. After 24 h of exposure, the results showed that none of the tested concentrations caused a significant decrease in cell viability (Figure S2).

Subsequently, all noncytotoxic concentrations were tested in the steatotic model induced by OA/PA. Among these, only the 50 μg/mL concentration consistently produced significant and reproducible protective effects, whereas lower concentrations were not effective (Figure S3). Therefore, 50 μg/mL CN was selected for all subsequent experiments.

We evaluated the lipid-lowering potential of the CN extract to reduce lipid accumulation in HepG2 cells treated with FFA mix of OA/PA. Intracellular lipid accumulation was visualized using ORO staining after 24h of treatment. As shown in Figures 4(a) and 4(b), while the extract alone did not induce steatotic effects ($p > 0.05$), OA/PA treatment led to a marked increase in size and intensity of lipid droplet accumulation within HepG2 cells compared to the control group, indicating a pronounced induction of NAFLD-like conditions ($159.29 \pm 2.01\%$ lipid accumulation, $p < 0.001$ vs. Ctrl). Conversely, the addition of the CN extract in the steatosis model significantly reduced lipid buildup ($122.78 \pm 0.64\%$ lipid accumulation, $p < 0.01$ vs. OA/PA), showing a potential relief effect on lipid accumulation.

In addition, the ability of the CN extract in reducing HepG2 lipid droplet accumulation has also been assessed in 3D cell culture systems (Figure 4(c)). As shown in Figure 4(d), the treatment with 50 μg/mL CN resulted in a reduction in the intracellular lipid content compared to OA/PA cells (OA/PA: $164.06 \pm 3.68\%$ lipid accumulation, $p < 0.001$ vs. Ctrl; OA/PA + CN: $123.96 \pm 7.37\%$ lipid accumulation, $p < 0.01$ vs. OA/PA). Thus, consistent with the results in the 2D model, the extract showed protective effects to spheroids as well.

To clarify the effects of CN on lipid metabolism, the mRNA expression levels were analyzed after 24 h of treatments. Lipogenic markers involved in promoting *de novo* FA synthesis and lipid storage in hepatocytes, contributing to steatosis markers, such as sterol regulatory element–binding protein 1c (SREBP-1c), FA synthase (FASN), and peroxisome proliferator–activated receptor gamma (PPARγ), were significantly increased in the OA/PA group compared to untreated cells (SREBP-1c, FASN, PPARγ: $p < 0.001$ vs. Ctrl) (Figure 4(e)). On the other hand, their expression significantly decreased in the coadministration with CN treatment (SREBP-1c, FASN, PPARγ: $p < 0.001$ vs. Ctrl).

Considering the phytochemical profile of the extract and previous literature reports [75–77], this effect may be attributed to the presence of compounds such as α-tocopherol, which has been shown to decrease SREBP-1c processing and lipogenic gene expression [78]. Polyunsaturated FA (PUFAs), particularly α-linolenic acid, are potent modulators of hepatic lipid metabolism. Omega-3s inhibit SREBP-1c, thereby reducing *de novo* lipogenesis, promoting FA β-oxidation, and decreasing triglyceride synthesis and secretion. They also upregulate PPARs and enhance the production of anti-inflammatory resolvins [79, 80]. On the contrary, the expression level of acetylated forkhead box O1 (FOXO1) and PPARα, two key transcriptional regulators involved in promoting FA oxidation and lipid catabolism, is increased in coadministration compared to FFA mix OA/PA, demonstrating the ability of the extract to activate genes involved

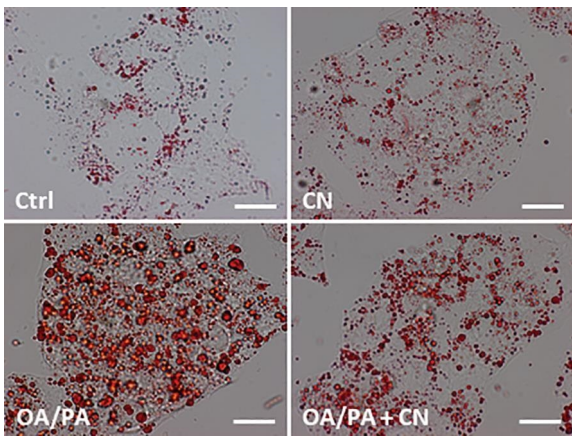

(a)

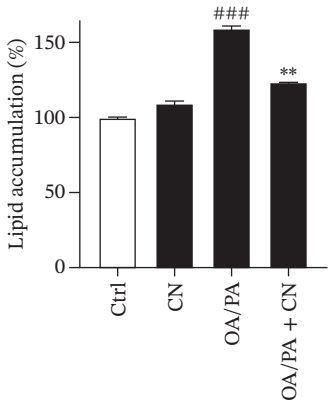

(b)

FIGURE 4 | (Continued)

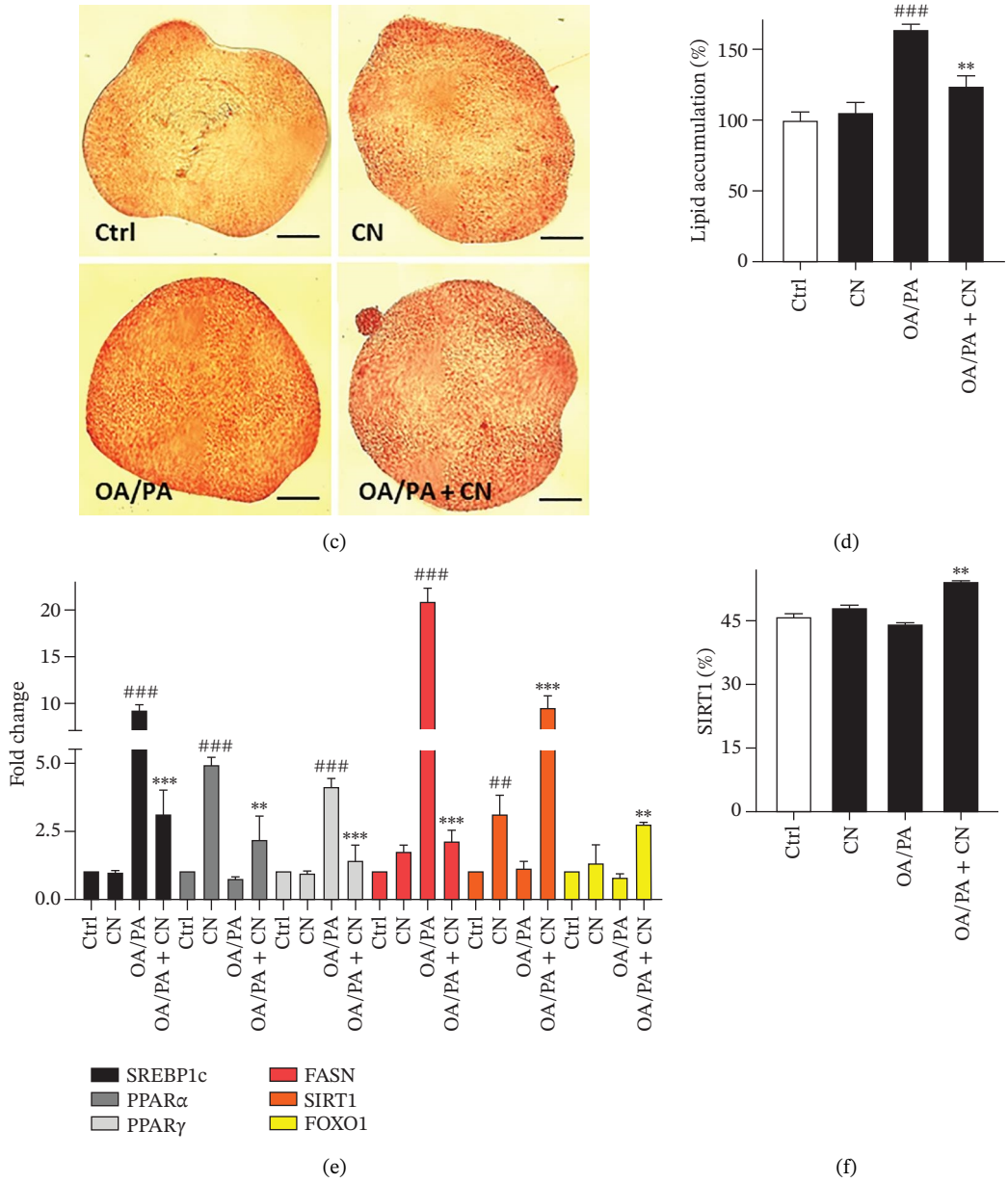

FIGURE 4 | Antisteatotic effects exerted by the CN extract. HepG2 cells are treated with OA/PA to induce NAFLD. The Ctrl group was treated with vehicles (1% BSA, 0.1% DMSO). The identified noncytotoxic concentration 50 μg/mL for the CN extract was used in subsequent experiments. (a) Representative images for the comparison of lipid accumulation in HepG2 cells based on ORO staining (magnification, 20×; scale bar: 100 μm). (b) Quantitative determination of lipid accumulation in 2D cells through spectrophotometric analysis. (c) Representative images of ORO-stained HepG2 spheroids (magnification, 20×; scale bar: 100 μm). (d) Quantitative determination of lipid accumulation in 3D cells through spectrophotometric analysis. (e) mRNA expression of lipid metabolism markers. (f) Quantitative determination of sirtuin 1 expression through flow cytometry analysis. Values are shown as mean ± SD ($n = 3$). ## and ### denote, respectively, $p < 0.01$ and $p < 0.001$ vs. Ctrl; ** and *** denote, respectively, $p < 0.01$ and $p < 0.001$ vs. OA/PA.

in lipid catabolism, reducing the steatotic phenotype (FOXO1, PPARα: $p < 0.01$ vs. OA/PA) (Figure 4(e)).

Moreover, SIRT1, a NAD^+-dependent deacetylase that can be activated by natural compounds and functions upstream of these genes, was also affected by the treatment (SIRT1: $p < 0.01$ vs. Ctrl, $p < 0.001$ vs. OA/PA), suggesting a potential role in orchestrating the overall modulation of lipid metabolic pathways (Figure 4(e)). To further confirm this hypothesis, the protein level of SIRT1 was evaluated through flow cytometry, highlighting an increase in SIRT1 expression after coadministration with CN in OA-/PA-treated cells in accordance with the gene expression (OA/PA + CN: $p < 0.01$ vs OA/PA) (Figure 4(f)).

3.3.2 | Antioxidant Activity of CN Extract

Treatment with OA and PA has been proven to be strong inducers of ROS and reactive nitrogen species (RNS), which play a key role in worsening the cellular microenvironment by amplifying oxidative stress caused by the intracellular accumulation of FA [81–83].

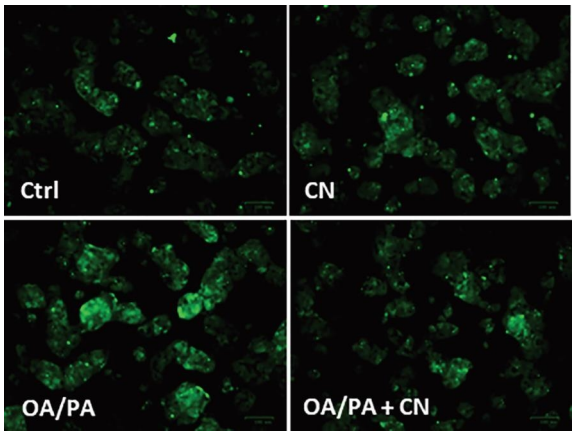

(a)

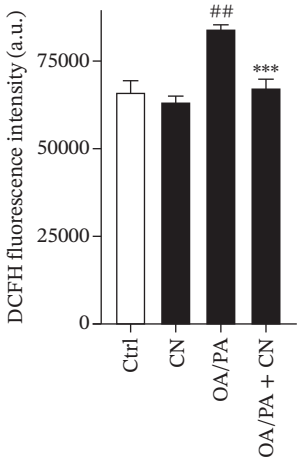

(b)

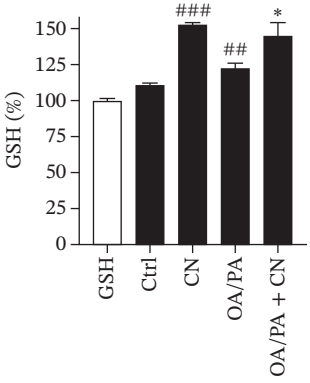

(c)

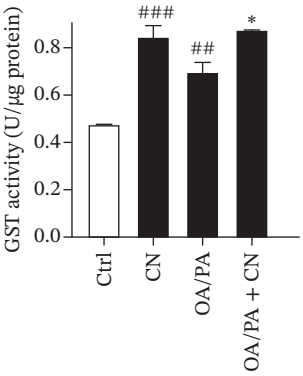

(d)

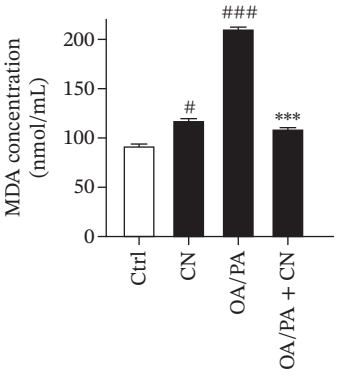

(e)

FIGURE 5 | (Continued)

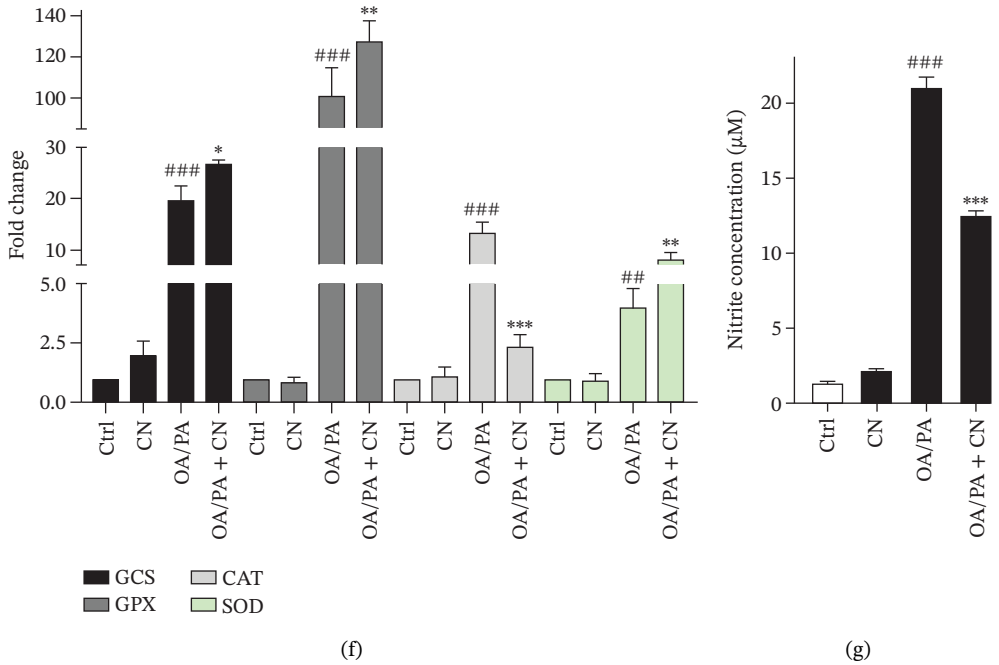

FIGURE 5 | Antioxidant properties shown by the CN extract. (a) Representative images for the comparison of ROS accumulation in HepG2 cells based on DCFH-DA staining (magnification, 20×. Scale bar: 100 μm). (b) Quantitative determination of intracellular ROS through spectrofluorometric analysis. (c) Quantitative analysis of intracellular GSH determination through spectrophotometric analysis. (d) Quantitative analysis of GST activity through spectrophotometric analysis. (e) Malondialdehyde quantification through spectrophotometric analysis. (f) mRNA expression of oxidative stress markers. (g) Quantitative analysis of extracellular nitrite. Values are shown as mean ± SD ($n = 3$). #, ##, and ### denote, respectively, $p < 0.05$, $p < 0.01$ and $p < 0.001$ vs. Ctrl; ∗, ∗∗, and ∗∗∗ denote, respectively, $p < 0.05$, $p < 0.01$ and $p < 0.001$ vs. OA/PA.

For these reasons, the antioxidant activity of the CN extract was evaluated. Experiments performed using DCFH-DA (Figures 5(a) and 5(b)) showed a significant reduction in intracellular ROS levels compared to the OA/PA treatment group ($p < 0.001$ vs. OA/PA), confirming that the decrease in intracellular lipid droplets contributes to restoring cellular redox balance. Furthermore, quantification of intracellular nitrite levels (Figure 5(g)) also showed a significant decrease compared to the FA mixture ($p < 0.001$ vs OA/PA).

Concurrently, levels of key antioxidant defenses, reduced GSH and GST (Figures 5(c) and 5(d)), were increased following CN treatment (GSH: 145.04 ± 9.02%, $p < 0.05$ vs. OA/PA; GST: 0.87 ± 0.03 U/μg protein, $p < 0.05$ vs. OA/PA), likely due to its combined antioxidant and antisteatotic effects, which help restore the cellular capacity to neutralize free radicals. By contrast, exposure to the FA mixture alone reduced GSH (122.31 ± 4.01%, $p < 0.01$ vs Ctrl) and GST (0.69 ± 0.04 U/μg protein, $p < 0.01$ vs Ctrl) levels, reflecting an overwhelmed and impaired antioxidant defense system under excessive oxidative stress.

Moreover, the CN extract significantly lowered MDA (CN: 108.34 ± 2.11 nmol/mL, $p < 0.001$ vs OA/PA; OA/PA: 210.94 ± 1.64 nmol/mL, $p < 0.001$ vs Ctrl) concentrations (Figure 5(e)), which reflects diminished lipid peroxidation and oxidative injury.

Real-time PCR analyses (Figure 5(f)) were performed to assess the expression of important antioxidant-related genes, including γ-glutamylcysteine synthetase (GCS), GSH peroxidase (GPx), superoxide dismutase (SOD), and catalase (CAT). In all cases, the gene expression trends mirrored those observed for GSH and GST levels: treatment with the FA mixture caused a modest downregulation compared to the CN-treated groups (GCS: $p < 0.05$ vs OA/PA; GPx: $p < 0.01$ vs OA/PA; CAT: $p < 0.001$ vs OA/PA; SOD: $p < 0.01$ vs OA/PA).

These results suggest that CN extract helps preserve and enhance the antioxidant defense pathways, counteracting the suppressive effect induced by OA/PA and supporting cellular redox homeostasis.

3.3.3 | Protective Effects of CN Extract on ER Stress and Mitochondrial Disfunction

The accumulation of intracellular lipids not only generates oxidative stress but also triggers ER stress, a key contributor to the development and progression of hepatic steatosis. Excessive lipid overload disrupts ER homeostasis by promoting protein misfolding and activating the unfolded protein response (UPR), which, if unresolved, can exacerbate cellular injury and lipotoxicity [84–86]. Moreover, ER stress can further propagate mitochondrial dysfunction, amplifying oxidative damage and energy imbalance.

To assess mitochondrial membrane potential, TMRE staining was performed: The results showed that fluorescence intensity was markedly decreased in cells treated with the FA mixture ($p < 0.01$ vs Ctrl), indicating mitochondrial dysfunction and depolarization. Conversely, cotreatment with the CN extract effectively restored TMRE fluorescence levels ($p < 0.01$ vs OA/PA), demonstrating a protective effect on mitochondrial integrity (Figures 6(a) and 6(b)).

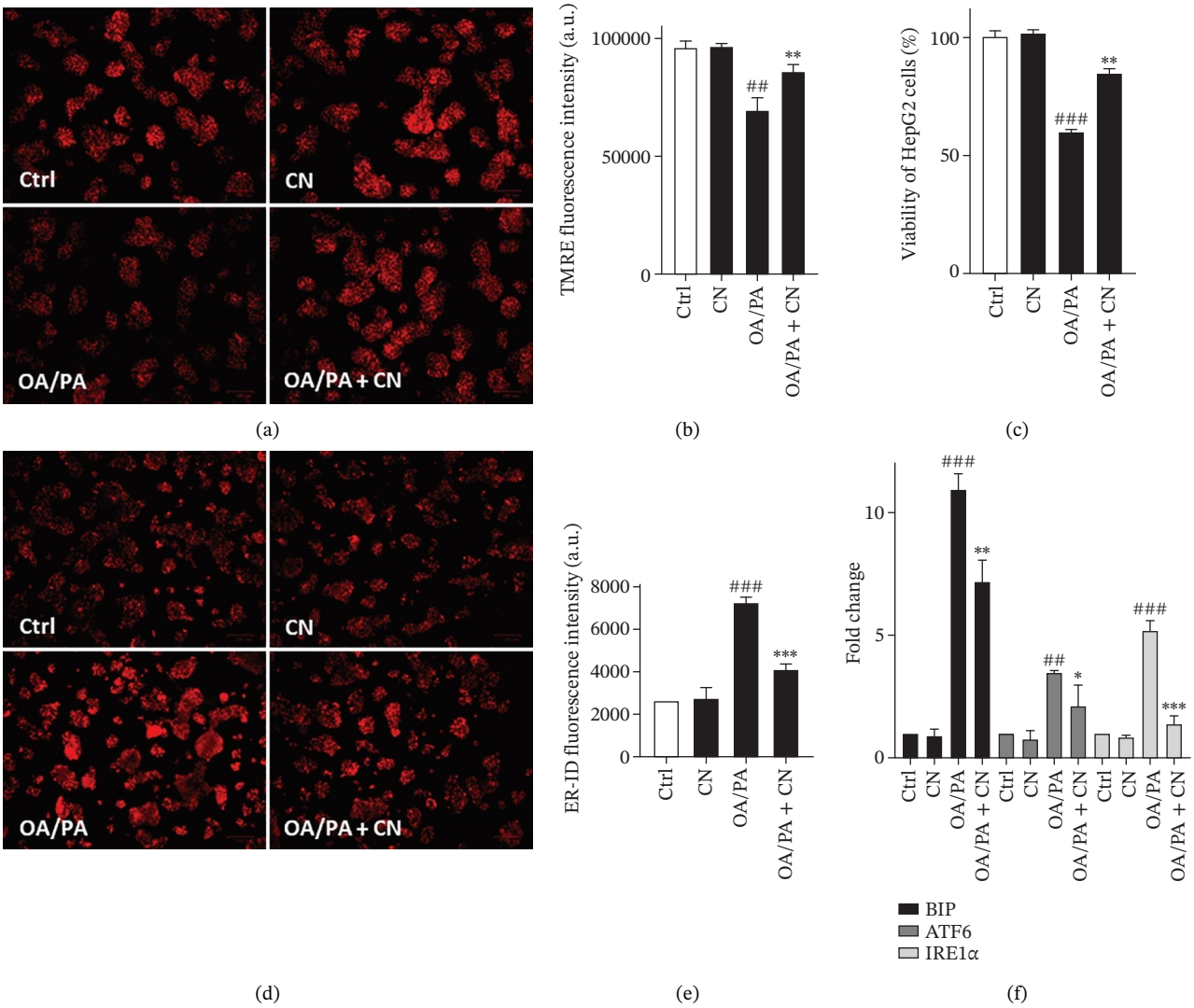

FIGURE 6 | Protective effects exerted by the CN extract against ER stress and mitochondrial disfunction. (a) Representative images for the comparison of mitochondrial permeability in HepG2 cells based on TMRE staining (magnification, 20×. Scale bar: 100 μm). (b) Quantitative analysis of TMRE fluorescence intensity related to mitochondrial permeability. (c) Mitochondrial metabolic activity tested by the MTT assay. (d) Representative images for the comparison of ER expansion in HepG2 cells based on ER-ID staining (magnification, 20×. Scale bar: 100 μm). (e) Quantitative analysis of ER-ID fluorescence intensity related to ER expansion. (f) mRNA expression of ER stress markers. Values are shown as mean ± SD ($n = 3$). ## and ### denote, respectively, $p < 0.01$ and $p < 0.001$ vs. Ctrl; ∗, ∗∗, and ∗∗∗ denote, respectively, $p < 0.05$, $p < 0.01$, and $p < 0.001$ vs. OA/PA.

These data were further confirmed by the MTT assay (Figure 6(c)), which showed that cellular mitochondrial activity was significantly reduced following OA/PA treatment (59.90 ± 1.32%, $p < 0.001$ vs Ctrl). Notably, treatment with the CN extract increased mitochondrial activity to 84.37 ± 2.44% ($p < 0.01$ vs. OA/PA), supporting its protective effect in maintaining mitochondrial function under lipotoxic stress.

The ER stress level was assessed using ER-ID staining (Figures 6(d) and 6(e)), which measures ER expansion and integrity. Cotreatment with the CN significantly reduced ER-ID fluorescence compared to the OA-/PA-treated group ($p < 0.001$ vs OA/PA). This reduction suggests that the extract helps alleviate the excessive protein-folding burden and misfolded protein accumulation.

In addition, the expression of key ER stress-related genes, including BiP ($p < 0.01$ vs OA/PA), ATF6, ($p < 0.05$ vs OA/PA), and IRE1α ($p < 0.001$ vs OA/PA), was evaluated by real-time PCR (Figure 6(f)). The results revealed that treatment with the extract markedly downregulated the transcription of these genes, further confirming its ability to mitigate ER stress and restore ER homeostasis under lipotoxic conditions. Given the abundance of flavonoids identified in the CN extract, their contribution to the observed protective effects appears highly plausible. Among them, quercetin stands out for its well-documented hepatoprotective activities. Previous studies have shown that quercetin reduces hepatic triglyceride accumulation and upregulates the spliced form of X-box binding protein 1 (XBP1), thereby enhancing VLDL assembly and promoting lipophagy through the activation of the IRE1α/XBP1 signaling axis. This dual regulation of lipid metabolism and ER homeostasis highlights the potential role of quercetin, and the flavonoid-rich fraction of the CN extract, in restoring hepatic metabolic balance under steatotic conditions [87, 88].

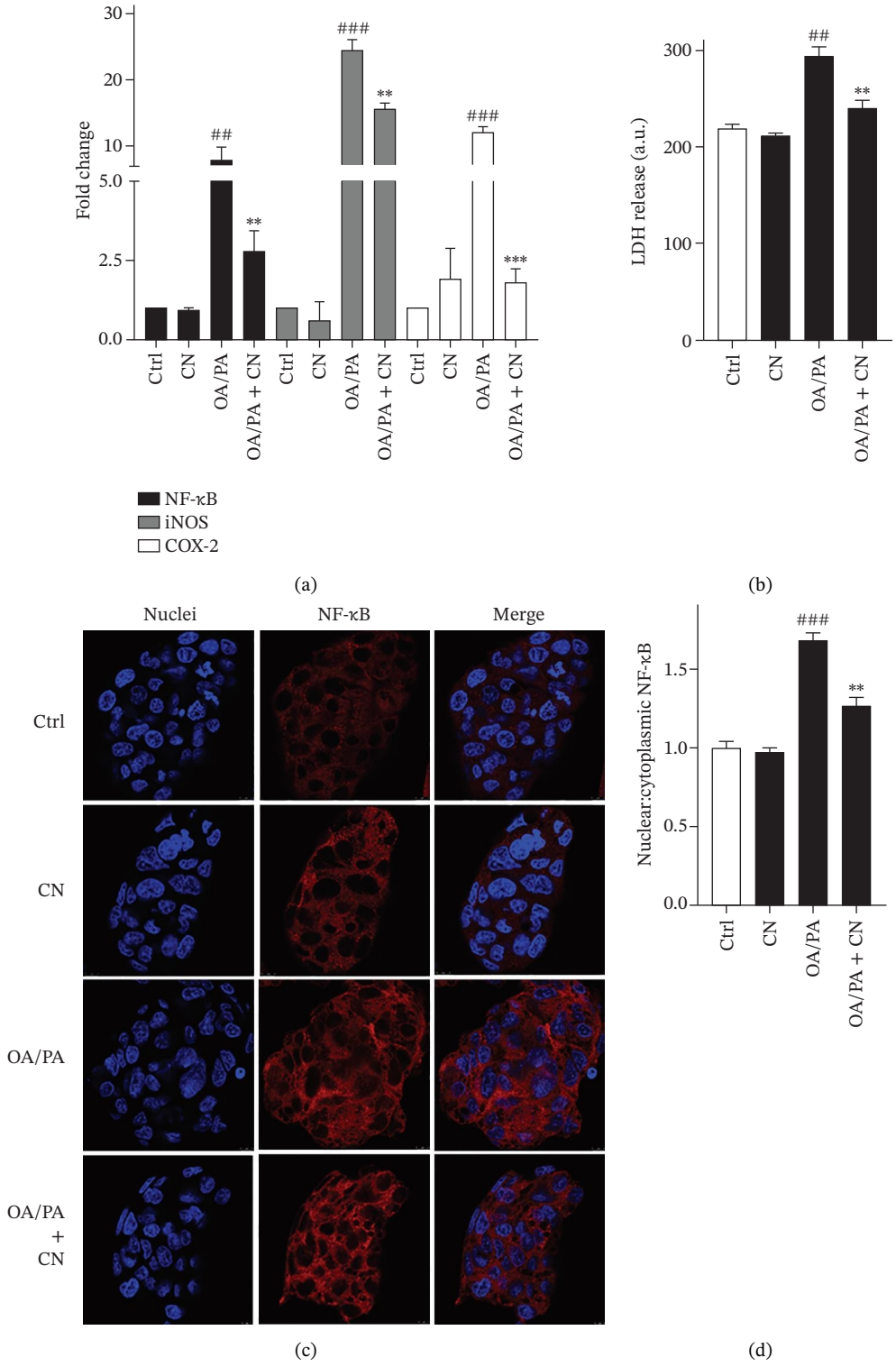

FIGURE 7 | Anti-inflammatory effects exerted by the CN extract. (a) mRNA expression of inflammatory markers. (b) Quantitative analysis of LDH release through luminescence assay. (c) Representative images of immunofluorescence staining of NF-κB (magnification, 63x. Scale bar: 10 μm). (d) Quantification of nuclear/cytoplasmic ratios of NF-κB staining. Values are shown as mean ± SD ($n = 3$). ## and ### denote, respectively, $p < 0.01$ and $p < 0.001$ vs. Ctrl; ** and *** denote, respectively, $p < 0.01$ and $p < 0.001$ vs. OA/PA.

3.3.4 | Anti-Inflammatory Properties of CN Extract

When steatosis occurs in hepatocytes, various inflammatory markers are activated and released. Therefore, we performed q-PCR to monitor the mRNA expression of inflammatory factors in OA/PA-induced HepG2 cells. Upon treatments, the mRNA expression levels of NF-κB, inducible nitric oxide synthase (iNOS), and cyclooxygenase-2 (COX-2) were significantly increased (NF-κB: $p < 0.01$ vs. Ctrl; iNOS, COX-2: $p < 0.001$ vs. Ctrl); however, these levels were markedly decreased following CN treatment

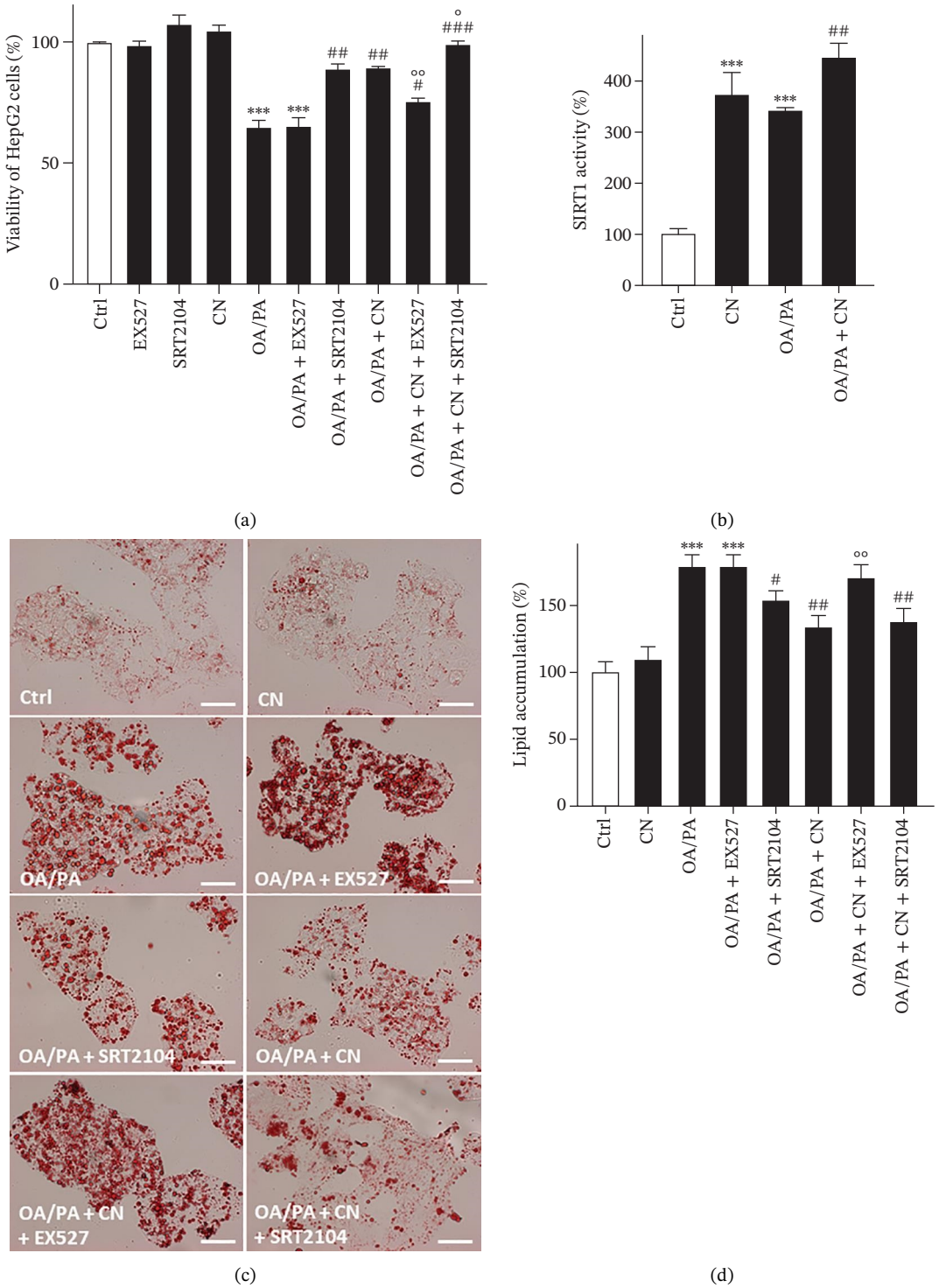

FIGURE 8 | Antisteatotic effects exerted by the CN extract are mediated by SIRT-1. (a) Mitochondrial metabolic activity tested by the MTT assay. (b) Sirtuin enzymatic activity tested on HepG2 cell lysates. (c) Representative images for the comparison of lipid accumulation in HepG2 cells based on ORO staining (magnification, 20×. Scale bar: 100 μm). (d) Quantitative determination of lipid accumulation in HepG2 cells through spectrophotometric analysis. Values are shown as mean ± SD ($n = 3$). #, ##, and ### denote, respectively, $p < 0.05$, $p < 0.01$, and $p < 0.001$ vs. Ctrl; *** denotes $p < 0.001$ vs. OA/PA; ∘, ∘∘ denote, respectively, $p < 0.05$ and $p < 0.01$ vs. OA/PA + CN.

(NF-κB, iNOS: $p < 0.01$ vs. OA/PA; COX-2: $p < 0.001$ vs. OA/PA) (Figure 7(a)). Several classes of bioactive compounds identified in the CN extract are known to influence the NF-κB signaling pathway, suggesting a potential contribution to its observed anti-inflammatory effects [15]. Among these, lutein has been shown to reduce lipid accumulation and modulate oxidative stress by lowering TNF-α, lipopolysaccharide (LPS), and NF-κB levels [89].

In addition, to corroborate the transcriptional modulation of proinflammatory genes observed by real-time PCR, we assessed LDH release as an indicator of cellular inflammation and injury.

Consistently, OA/PA exposure led to a significant increase in LDH release compared to control cells ($p < 0.01$ vs. Ctrl), reflecting lipid-induced cytotoxicity and inflammation. Notably, CN treatment markedly reduced LDH levels ($p < 0.01$ vs. OA/PA) (Figure 7(b)). Furthermore, confocal microscopy confirmed a reduced nuclear translocation of NF-κB in CN-treated cells (1.26-fold increase; $p < 0.01$ vs OA/PA) compared to OA/PA (1.68-fold increase; $p < 0.001$ vs. Ctrl), supporting its role in mitigating inflammatory signaling at both transcriptional and functional levels (Figure 7(c)).

3.3.5 | Role of SIRT1 in Hepatoprotective Properties of CN

To elucidate the contribution of SIRT1 to the protective effects of CN against FA-induced lipotoxicity, we performed a set of experiments using the selective SIRT1 inhibitor EX527 and the activator SRT2104 [28, 90] (Figure 8). Treatment of HepG2 cells with OA/PA markedly decreased cell viability ($p < 0.001$ vs Ctrl), whereas coincubation with CN extract restored cell viability to near-control levels ($p < 0.01$ vs OA/PA). The selective SIRT1 activator SRT2104 reproduced this effect ($p < 0.01$ vs OA/PA), while the inhibitor EX527 prevented the CN-mediated improvement, maintaining low viability ($p < 0.001$ vs Ctrl). When OA/PA were administered together with CN and EX527, cell viability was significantly reduced compared with OA/PA + CN alone ($p < 0.01$ vs OA/PA + CN), whereas SRT2104 further enhanced the protective action of CN ($p < 0.05$ vs OA/PA + CN), indicating a potential additive interaction between the extract and SIRT1 activation and confirming that SIRT1 is at least partially involved in the hepatoprotective mechanism elicited by CN. Consistently, the assessment of SIRT1 enzymatic activity revealed that its levels, while not markedly suppressed by OA/PA alone, were further increased upon CN cotreatment ($p < 0.01$ vs OA/PA), following a trend comparable to that observed for SIRT1 protein expression (Figure 4(f)). This finding further supports that the protective effects observed in the cell viability assay are associated with a direct enhancement of SIRT1 activity under lipotoxic conditions.

CARs and CHLs may contribute to the observed increase in SIRT1 expression.

These pigment classes have been widely reported to modulate key molecular mechanisms implicated in the progression of NAFLD. For instance, fucoxanthin has been reported to attenuate NAFLD by regulating lipid metabolism, oxidative stress, and inflammation through activation of the AMP-activated protein kinase/nuclear factor erythroid 2–related factor 2/Toll-like receptor 4 (AMPK/Nrf2/TLR4) signaling pathway [91]. Similarly, zeaxanthin downregulated p53 expression and modulated its downstream targets, including GPx4, solute carrier family 7 member 11 (SLC7A11), spermidine/spermine N1-acetyltransferase 1 (SAT1), and arachidonate 15-lipoxygenase (ALOX15), thereby reducing cellular lipid peroxidation [92]. Particular attention should be given to β-cryptoxanthin, which markedly reduces hepatic fat accumulation by inducing SIRT1 activity and upregulating peroxisome PPARγ coactivator 1-alpha (PGC1α) and PPARα expression. It was demonstrated that β-cryptoxanthin supplementation also decreased acetylated FOXO1 levels, indicating an increase in SIRT1 enzymatic activity. Through SIRT1-mediated deacetylation of SREBP-1c and activation of PGC1α, β-cryptoxanthin (BCX) effectively stimulates the SIRT1/PGC1α/PPARα signaling cascade, suppresses hepatic lipogenesis, and ultimately mitigates hepatic steatosis [93, 94].

ORO staining further substantiated the findings obtained from the cell viability assay (Figures 8(a) and 8(b)). As expected, exposure to OA/PA led to marked intracellular lipid accumulation ($p < 0.001$ vs Ctrl), whereas treatment with CN partially reduced the number and size of lipid droplets ($p < 0.01$ vs OA/PA). A similar attenuation of steatosis was observed with SRT2104 ($p < 0.05$ vs OA/PA), while EX527 largely preserved the steatotic effect of FA ($p < 0.01$ vs Ctrl). When OA/PA were coadministered with CN and EX527, lipid accumulation increased compared with OA/PA + CN ($p < 0.01$ vs OA/PA + CN), restoring the lipid burden to levels close to those induced by OA/PA alone. On the other hand, SRT2104 produced a reduction in lipid droplets comparable to that achieved by CN, and their combination did not further enhance this effect, suggesting a mainly additive contribution of SIRT1 activation to the action of CN, possibly reflecting a ceiling effect once SIRT1 activation reaches a sufficient level. Interestingly, unlike the MTT results where the combination of CN and SRT2104 slightly outperformed OA/PA + CN, the lipid droplet content did not decrease further, suggesting that while SIRT1 activation may still support cell viability, its contribution to CN-mediated lipid clearance reaches a plateau beyond which additional stimulation does not translate into greater antisteatotic benefit.

Overall, these results mirror the pattern observed in the MTT assay and provide further confirmation that SIRT1 plays at least a partial role in mediating the antisteatotic action of CN. Spectrophotometric quantification of extracted ORO dye corroborated the microscopic observations, confirming that CN significantly reduces lipid content through a mechanism that involves SIRT1-dependent modulation of lipid storage in hepatocytes challenged with FFAs (Figures 8(c) and 8(d)).

4 | Conclusions

Our findings demonstrate that the CN extract exerts a potent protective effect against lipotoxicity-induced cellular dysfunction in a NAFLD HepG2 model. CN treatment effectively mitigated intracellular lipid accumulation in both 2D and 3D culture systems, by downregulating lipogenic genes and upregulating lipid catabolism markers. In parallel, the extract restored redox homeostasis, as evidenced by reduced ROS and RNS levels, enhanced antioxidant defenses, and increased the expression of key antioxidant enzymes, highlighting its ability to counteract oxidative stress.

Moreover, the CN extract alleviated ER stress and preserved mitochondrial integrity, as shown by reduced ER-ID fluorescence, decreased expression of ER stress markers, and restoration of mitochondrial membrane potential and function. A key element underlying these effects was the activation of SIRT1, a master regulator of lipid metabolism, mitochondrial function, and oxidative/ER stress responses. CN markedly increased SIRT1 expression and activity, and pharmacological modulation with the selective inhibitor EX527 and the activator SRT2104 confirmed the pivotal contribution of SIRT1 to the antisteatotic and cytoprotective actions of CN.

Finally, CN demonstrated anti-inflammatory properties by reducing the expression of proinflammatory genes, limiting NF-κB nuclear translocation, and attenuating LDH release.

Collectively, these results suggest that CN extract counteracts the deleterious effects of FFA-induced lipotoxicity through a multitarget mechanism in which SIRT1 activation played a pivotal role, integrating the modulation of lipid metabolism, oxidative and ER stress, mitochondrial dysfunction, and inflammation. This highlights its potential as a promising candidate for further investigation as a sustainable nutraceutical for the prevention or adjunct treatment of NAFLD and related metabolic disorders.

Funding

This project was funded under the National Recovery and Resilience Plan (NRRP), Mission 4 Component 2 Investment 1.4—Call for tender No. 3138 of December 16, 2021, rectified by Decree n.3175 of December 18, 2021, of Italian Ministry of University and Research funded by the European Union–NextGenerationEU. Award No.: Project code CN_00000033, Concession Decree No.: 1034 of June 17, 2022 adopted by the Italian Ministry of University and Research, CUP: D43C22001260001, Project title "National Biodiversity Future Center—NBFC."

Conflicts of Interest

The authors declare no conflicts of interest.

Data Availability Statement

The original contributions presented in this study are included in the article/Supporting Information. Further inquiries can be directed to the corresponding authors.

References

1. V. Puri, M. Nagpal, I. Singh, et al., "A Comprehensive Review on Nutraceuticals: Therapy Support and Formulation Challenges," *Nutrients* 14, no. 4637 (2022): 4637, https://doi.org/10.3390/nu14214637.

2. S. Chandra, S. Saklani, P. Kumar, B. Kim, and H. D. M. Coutinho, "Nutraceuticals: Pharmacologically Active Potent Dietary Supplements," *BioMed Research International* 2022, no. 1 (2022): 2051017, https://doi.org/10.1155/2022/2051017.

3. Y. Takefuji, "Nutraceuticals: a Promising, yet Unregulated Frontier in Healthcare," *European Journal of Clinical Nutrition* 79, no. 5 (2024): 413–418, https://doi.org/10.1038/s41430-024-01557-y.

4. P. Marino, G. Pepe, M. G. Basilicata, et al., "Potential Role of Natural Antioxidant Products in Oncological Diseases," *Antioxidants* 12, no. 704 (2023): 704, https://doi.org/10.3390/antiox12030704.

5. M. Vacca, E. M. Sommella, M. Liso, et al., "Anthocyanins from Purple Corn Affect Gut Microbiota and Metabolome in Inflammatory Bowel Disease Patients Under Infliximab Infusion: the Sicura Pilot Study," *Food Science and Human Wellness* 13, no. 6 (2024): 3536–3543, https://doi.org/10.26599/FSHW.2023.9250036.

6. M. Del Ben, L. Polimeni, F. Baratta, D. Pastori, and F. Angelico, "The Role of Nutraceuticals for the Treatment of Non-alcoholic Fatty Liver Disease," *British Journal of Clinical Pharmacology* 83, no. 1 (2017): 88–95, https://doi.org/10.1111/bcp.12899.

7. B. Sosnowska, P. Penson, and M. Banach, "The Role of Nutraceuticals in the Prevention of Cardiovascular Disease," *Cardiovascular Diagnosis and Therapy* 7, no. 1 (2017): S21–S31, https://doi.org/10.21037/cdt.2017.03.20.

8. G. Augimeri, F. I. Montalto, C. Giordano, et al., "Nutraceuticals in the Mediterranean Diet: Potential Avenues for Breast Cancer Treatment," *Nutrients* 13, no. 8 (2021): 2557, https://doi.org/10.3390/nu13082557.

9. N. Abderrrezag, G. Domínguez-Rodríguez, L. Montero, and J. A. Mendiola, "Nutraceutical Potential of Mediterranean agri-food Waste and Wild Plants: Green Extraction and Bioactive Characterization," in *Advances in Food and Nutrition Research*, ed. F. Toldrá, 114 (Academic Press, 2025), 1–95, https://doi.org/10.1016/bs.afnr.2024.09.001.

10. G. Aquino, M. G. Basilicata, C. Crescenzi, et al., "Optimization of microwave-assisted Extraction of Antioxidant Compounds from Spring Onion Leaves Using Box–Behnken Design," *Scientific Reports* 13, no. 1 (2023): 14923, https://doi.org/10.1038/s41598-023-42303-x.

11. C. Zhang and M. Yang, "Molecular Targets Regulating Endoplasmic reticulum-mitochondria Crosstalk for NAFLD Treatment," *Exploration of Medicine* 2 (2021): 494–510, https://doi.org/10.37349/emed.2021.00066.

12. N. Alkhouri, L. J. Dixon, and A. E. Feldstein, "Lipotoxicity in Nonalcoholic Fatty Liver Disease: Not all Lipids are Created Equal," *Expert Review of Gastroenterology & Hepatology* 3, no. 4 (2009): 445–451, https://doi.org/10.1586/egh.09.32.

13. S. Novi, V. Vestuto, P. Campiglia, N. Tecce, A. Bertamino, and M. F. Tecce, "Anti-Angiogenic Effects of Natural Compounds in diet-associated Hepatic Inflammation," *Nutrients* 15, no. 12 (2023): 2748, https://doi.org/10.3390/nu15122748.

14. D. Meng, F. Zhang, W. Yu, et al., "Biological Role and Related Natural Products of SIRT1 in Nonalcoholic Fatty Liver," *Diabetes, Metabolic Syndrome and Obesity* 16 (2023): 4043–4064, https://doi.org/10.2147/DMSO.S437865.

15. L. M. Lewis Lujan, M. F. McCarty, J. C. Galvez Ruiz, S. Trujillo Lopez, and S. B. Iloki-Assanga, "Nutraceutical and Dietary Measures with Potential for preventing/controlling Non-alcoholic Fatty Liver Disease and Its Complications," *Human Nutrition & Metabolism* 37 (2024): 200281, https://doi.org/10.1016/j.hnm.2024.200281.

16. E. Trigueros, Ó. Benito-Román, A. P. Oliveira, et al., "Onion (*Allium cepa* L.) Skin Waste Valorization: Unveiling the Phenolic Profile and Biological Potential for the Creation of Bioactive Agents Through Subcritical Water Extraction," *Antioxidants* 13, no. 2 (2024): 205, https://doi.org/10.3390/antiox13020205.

17. A. S. Bedir, R. S. Almasri, Y. O. Azar, R. E. Elnady, and S. M. Al Raish, "Exploring the Therapeutic Potential of *Allium cepa* and *Allium sativum* Extracts: Current Strategies, Emerging Applications, and Sustainability Utilization," *Biology* 14, no. 8 (2025): 1088, https://doi.org/10.3390/biology14081088.

18. H. J. Lee, I. Y. Lee, J. H. Park, and N. Joo, "Comparison of Phytochemicals and Antioxidant Activities of Onion (*Allium cepa L.*) Bulbs, Onion Leaves, and Green Onion (*Allium fistulosum L.*) Leaves," *Journal of Food Science and Nutrition* 28, no. 1 (2025): 2507121, https://doi.org/10.1080/10942912.2025.2507121.

19. D. Kurnia, D. Ajiati, L. Heliawati, and D. Sumiarsa, "Antioxidant Properties and Structure-Antioxidant Activity Relationship of *Allium* Species Leaves," *Molecules* 26, no. 23 (2021): 7175, https://doi.org/10.3390/molecules26237175.

20. G. Aquino, E. M. Sommella, E. Salviati, et al., "Advancing Profiling of Secondary Antioxidant Metabolites in Allium cepa PDO Leaf Extract: Online 2D-LC–HRMS with Pre-column DPPH Assay," *Journal of Chromatography A* 1749 (2025): 465877, https://doi.org/10.1016/j.chroma.2025.465877.

21. V. Imeneo, A. De Bruno, A. Piscopo, R. Romeo, and M. Poiana, "Valorization of 'Rossa Di Tropea' Onion Waste Through Green Recovery Techniques of Antioxidant Compounds," *Sustainability* 14, no. 8 (2022): 4387, https://doi.org/10.3390/su14084387.

22. R. Schmid, S. Heuckeroth, A. Korf, et al., "Integrative Analysis of Multimodal Mass Spectrometry Data in Mzmine 3," *Nature Biotechnology* 41, no. 4 (2023): 447–449, https://doi.org/10.1038/s41587-023-01690-2.

23. C. Brungs, R. Schmid, S. Heuckeroth, et al., "Msnlib: Efficient Generation of Open multi-stage Fragmentation Mass Spectral Libraries," *Nature Methods* 22, no. 10 (2025): 2028–2031, https://doi.org/10.1038/s41592-025-02813-0.

24. M. L. Way, J. E. Jones, D. S. Nichols, R. G. Dambergs, and N. D. Swarts, "A Comparison of Laboratory Analysis Methods for Total Phenolic Content of Cider," *Beverages* 6, no. 3 (2020): 55, https://doi.org/10.3390/beverages6030055.

25. H. Wang, Y. Zhu, D. Xie, et al., "The Effect of Microwave Radiation on the Green Color Loss of Green Tea Powder," *Foods* 11, no. 16 (2022): 2540, https://doi.org/10.3390/foods11162540.

26. D. Šamec, M. Bogović, D. Vincek, J. Martinčić, and B. Salopek-Sondi, "Assessing the Authenticity of the White Cabbage (*Brassica oleracea* Var. *Capitata* F. *Alba*) Cv. 'Varaždinski' by Molecular and Phytochemical Markers," *Food Research International* 60 (2014): 266–272, https://doi.org/10.1016/j.foodres.2013.07.015.

27. H. Noreen, N. Semmar, M. Farman, and J. S. O. McCullagh, "Measurement of Total Phenolic Content and Antioxidant Activity of Aerial Parts of *Coronopus Didymus*," *Asian Pacific Journal of Tropical Medicine* 10, no. 8 (2017): 792–801, https://doi.org/10.1016/j.apjtm.2017.07.024.

28. Y. Lei, X.-L. Ma, T. Liu, et al., "Lactucin Ameliorates FFA-Induced Steatosis in HepG2 Cells by Modulating Mitochondrial Homeostasis Through the SIRT1/PGC-1α Axis," *Heliyon* 10, no. 21 (2024): e39890, https://doi.org/10.1016/j.heliyon.2024.e39890.

29. T. E. Maseko, M. Elkalaf, E. Peterová, et al., "Comparison of Heparg and HepG2 Cell Lines to Model Mitochondrial Respiratory Adaptations in NAFLD," *International Journal of Molecular Medicine* 53, no. 2 (2024): 18, https://doi.org/10.3892/ijmm.2023.5342.

30. J. Mun, S. Kim, H. G. Yoon, et al., "Water Extract of Curcuma longa L. Ameliorates Non-alcoholic Fatty Liver Disease," *Nutrients* 11, no. 10 (2019): 2536, https://doi.org/10.3390/nu11102536.

31. H. Dhami-Shah, R. Vaidya, S. Udipi, et al., "Picroside II Attenuates Fatty Acid Accumulation in HepG2 Cells via Modulation of Fatty Acid Uptake and Synthesis," *Clinical and Molecular Hepatology* 24, no. 1 (2018): 77–87, https://doi.org/10.3350/cmh.2017.0039.

32. V. Vestuto, T. Ciaglia, S. Musella, et al., "A Comprehensive in Vitro Characterization of a New Class of Indole-based Compounds Developed as Selective Haspin Inhibitors," *Journal of Medicinal Chemistry* 8, no. 15 (2024): 12711–12734, https://doi.org/10.1021/acs.jmedchem.4c00718.

33. E. Colarusso, G. Lauro, M. Potenza, et al., "5-methyl-2-carboxamidepyrrole-based Novel Dual mPGES-1/sEH Inhibitors as Promising Anticancer Candidates," *Archiv der Pharmazie* 358, no. 1 (2025): e2400708, https://doi.org/10.1002/ardp.202400708.

34. V. Vestuto, M. Conte, M. Vietri, et al., "Multiomic Profiling and Neuroprotective Bioactivity of Salvia Hairy root-derived Extracellular Vesicles in a Cellular Model of Parkinson's disease," *International Journal of Nanomedicine* 11 (2024): 9373–9393, https://doi.org/10.2147/ijn.s479959.

35. C. M. Wu, Y. L. Cheng, Y. H. Dai, M. F. Chen, and C. C. Wang, "α-tocopherol Protects Keratinocytes Against Ultraviolet A Irradiation by Suppressing Glutathione Depletion, Lipid Peroxidation and Reactive Oxygen Species Generation," *Biomedical Reports* 2, no. 3 (2014): 419–423, https://doi.org/10.3892/br.2014.236.

36. P. K. Issac, A. Guru, M. Velayutham, et al., "Oxidative Stress Induced Antioxidant and Neurotoxicity Demonstrated in in Vivo Zebrafish Embryo or Larval Model and Their Normalization due to Morin Showing Therapeutic Implications," *Life Sciences* 283 (2021): 119864, https://doi.org/10.1016/j.lfs.2021.119864.

37. P. D. Moore, C. G. Yedjou, and P. B. Tchounwou, "Malathion-Induced Oxidative Stress, Cytotoxicity, and Genotoxicity in Human Liver Carcinoma (Hepg2) Cells," *Environmental Toxicology* 25, no. 3 (2010): 221–226, https://doi.org/10.1002/tox.20492.

38. M. R. Miranda, M. G. Basilicata, V. Vestuto, et al., "Anticancer Therapies Based on Oxidative Damage: Lycium barbarum Inhibits the Proliferation of MCF-7 Cells by Activating Pyroptosis Through Endoplasmic Reticulum Stress," *Antioxidants* 13, no. 6 (2024): 708, https://doi.org/10.3390/antiox13060708.

39. M. J. Kim, "Betaine Enhances the Cellular Survival via Mitochondrial Fusion and Fission Factors, MFN2 and DRP1," *Animal Cells and Systems* 22, no. 5 (2018): 289–298, https://doi.org/10.1080/19768354.2018.1512523.

40. M. R. Miranda, C. Montano, V. Golino, et al., "Integrated Proteomics Highlights Functional Activation Induced by advanced-platelet Rich Fibrin plus (A-PRF+) in Primary Equine Fibroblasts," *Scientific Reports* 23, no. 1 (2025): 18021, https://doi.org/10.1038/s41598-025-01820-7.

41. M. Li, M. Zhang, Z. L. Zhang, et al., "Induction of Apoptosis by Berberine in Hepatocellular Carcinoma HepG2 Cells via Downregulation of NF-κB," *Oncology Research* 25, no. 2 (2017): 233–239, https://doi.org/10.3727/096504016X14742891049073.

42. I. Kim, M. L. Kyun, H. Jung, et al., "In Vitro Nonalcoholic Fatty Liver Disease Model Elucidating the Effect of Immune Environment on Disease Progression and Alleviation," *ACS Omega* 9, no. 23 (2024): 25094–25105, https://doi.org/10.1021/acsomega.4c02433.

43. P. Pingitore, K. Sasidharan, M. Ekstrand, S. Prill, D. Lindén, and S. Romeo, "Human Multilineage 3D Spheroids as a Model of Liver Steatosis and Fibrosis," *International Journal of Molecular Sciences* 20, no. 7 (2019): 1629, https://doi.org/10.3390/ijms20071629.

44. B. K. Das, R. M. Knott, and P. C. Gadad, "Metformin and Asarone Inhibit HepG2 Cell Proliferation in a High Glucose Environment by Regulating AMPK and Akt Signaling Pathway," *Future Journal of Pharmaceutical Sciences* 7, no. 1 (2021): 43, https://doi.org/10.1186/s43094-021-00193-8.

45. M. Buonocore, M. Grimaldi, A. Santoro, et al., "Exploiting the Features of Short Peptides to Recognize Specific Cell Surface Markers," *International Journal of Molecular Sciences* 24, no. 21 (2023): 15610, https://doi.org/10.3390/ijms242115610.

46. J. W. Yang, Y. Zou, J. Chen, et al., "Didymin Alleviates Metabolic dysfunction-associated Fatty Liver Disease (MAFLD) via the Stimulation of Sirt1-mediated Lipophagy and Mitochondrial Biogenesis," *Journal of Translational Medicine* 21, no. 1 (2023): 921, https://doi.org/10.1186/s12967-023-04790-4.

47. I. Tedesco, V. Carbone, C. Spagnuolo, P. Minasi, and G. L. Russo, "Identification and Quantification of Flavonoids from Two Southern Italian Allium cepa L. cultivars and Their Capacity to Protect Erythrocytes from Oxidative Stress," *Journal of Agricultural and Food Chemistry* 63, no. 21 (2015): 5229–5238, https://doi.org/10.1021/acs.jafc.5b01206.

48. D. Yang, F. R. Dunshea, and H. A. R. Suleria, "LC-ESI-QTOF/MS Characterization of Australian Herbs and Spices (Garlic, Ginger, and Onion) and Their Antioxidant Activity," *Journal of Food Processing and Preservation* 44, no. 7 (2020): https://doi.org/10.1111/jfpp.14497.

49. L. Campone, R. Celano, A. L. Piccinelli, et al., "Response Surface Methodology to Optimize Supercritical CO_2 Extraction of Brown Onion Skin as a Source of Nutraceutical Compounds," *Food Chemistry* 269 (2018): 495–502, https://doi.org/10.1016/j.foodchem.2018.07.042.

50. W. M. Dabeek, N. Kovinich, C. Walsh, and M. Ventura Marra, "Characterization and Quantification of Major Flavonol Glycosides in Ramps (Allium tricoccum)," *Molecules* 24, no. 18 (2019): 3281, https://doi.org/10.3390/molecules24183281.

51. T. Soininen, *Metabolite Profiling of Allium Species by Using Modern Spectrometric Methods*, 236 (University of Eastern Finland, Dissertations in Health Sciences, 2014).

52. S. Schmidt, M. Zietz, M. Schreiner, S. Rohn, L. W. Kroh, and A. Krumbein, "Identification of Complex, Naturally Occurring Flavonoid Glycosides in Kale by HPLC-DAD/ESI-MS^n," *Rapid Communications in*

Mass Spectrometry 24, no. 14 (2010): 2009–2022, https://doi.org/10.1002/rcm.4605.

53. S. Zheng, J. Szymański, N. Shahaf, et al., "Metabolic Diversity in Wild and Cultivated Brassica rapa Subspecies," *Frontiers in Molecular Biosciences* 9 (2022): 953189, https://doi.org/10.3389/fmolb.2022.953189.

54. M. J. Conroy, R. M. Andrews, S. Andrews, et al., "LIPID MAPS: Update to Databases and Tools for the Lipidomics Community," *Nucleic Acids Research* 52, no. D1 (2024): D1677–D1682, https://doi.org/10.1093/nar/gkad896.

55. M. A. Farag, S. E. Ali, R. H. Hodaya, et al., "Phytochemical Profiles and Antimicrobial Activities of Allium cepa Red Cv. and A. sativum Subjected to Different Drying Methods," *Molecules* 22, no. 5 (2017): 761, https://doi.org/10.3390/molecules22050761.

56. S. Lachowicz, J. Oszmiański, and R. Wiśniewski, "Determination of Triterpenoids, Carotenoids, Chlorophylls, and Antioxidant Capacity in Allium ursinum L. at Different Times of Harvesting and Anatomical Parts," *European Food Research and Technology* 244, no. 7 (2018): 1269–1280, https://doi.org/10.1007/s00217-018-3042-3.

57. K. Chen, J. J. Ríos, A. Pérez-Gálvez, and M. Roca, "Comprehensive Chlorophyll Composition in the Main Edible Seaweeds," *Food Chemistry* 228 (2017): 625–633, https://doi.org/10.1016/j.foodchem.2017.02.036.

58. A. Wojdyło, P. Nowicka, K. Tkacz, and I. P. Turkiewicz, "Sprouts Vs. Microgreens as Novel Functional Foods: Variation of Nutritional and Phytochemical Profiles and Their in Vitro Bioactive Properties," *Molecules* 25, no. 20 (2020): 4648, https://doi.org/10.3390/molecules25204648.

59. A. Wojdyło, P. Nowicka, K. Tkacz, and I. P. Turkiewicz, "Fruit Tree Leaves as Unconventional and Valuable Source of Chlorophyll and Carotenoid Compounds Determined by LC-PDA-qTOF-ESI-MS," *Food Chemistry* 349 (2021): 129156, https://doi.org/10.1016/j.foodchem.2021.129156.

60. S. C. Huang, C. F. Hung, W. B. Wu, and B. H. Chen, "Determination of Chlorophylls and Their Derivatives in *Gynostemma pentaphyllum* Makino by Liquid chromatography–mass Spectrometry," *Journal of Pharmaceutical and Biomedical Analysis* 48, no. 1 (2008): 105–112, https://doi.org/10.1016/j.jpba.2008.05.009.

61. H. Lohani, A. Kumar, V. Bidarakundi, L. Agrawal, S. Z. Haider, and N. K. Chauhan, "Identification of Fatty Acids, Amides and Cinnamic Acid Derivatives in supercritical-CO_2 Extracts of Cinnamomum tamala Leaves Using UPLC-Q-TOF-MSE with Chemometrics," *Molecules* 29, no. 16 (2024): 3760, https://doi.org/10.3390/molecules29163760.

62. Q. Li, X. Liang, L. Zhao, et al., "UPLC-Q-Exactive Orbitrap/MS-based Lipidomics Characterization of Bee Pollen Extracts and Their in Vitro Anti-inflammatory Properties," *Journal of Agricultural and Food Chemistry* 65, no. 32 (2017): 6848–6860, https://doi.org/10.1021/acs.jafc.7b02285.

63. E. Alves, T. Melo, M. P. Barros, M. R. M. Domingues, and P. Domingues, "Lipidomic Profiling of Olive Fruits (*Olea europaea* L.) for Their Valorisation as Functional Food: Identification of Triacylglycerols and Polar Lipids," *Molecules* 24, no. 14 (2019): 2555, https://doi.org/10.3390/molecules24142555.

64. O. Montero, M. Velasco, J. Miñón, et al., "Differential Membrane Lipid Profiles and Vibrational Spectra of Three Edaphic Algae and One Cyanobacterium," *International Journal of Molecular Sciences* 22, no. 20 (2021): 11277, https://doi.org/10.3390/ijms222011277.

65. Y. J. Lee, R. C. Leverence, E. A. Smith, J. S. Valenstein, K. Kandel, and B. G. Trewyn, "High-Throughput Analysis of Algal Crude Oils Using high-resolution Mass Spectrometry," *Lipids* 48, no. 3 (2013): 297–305, https://doi.org/10.1007/s11745-013-3757-7.

66. S. Lewenza, R. Falsafi, M. Bains, et al., "The Olsa Gene Mediates Synthesis of an Ornithine Lipid in *Pseudomonas aeruginosa* Under phosphate-limiting Conditions," *FEMS Microbiology Letters* 320, no. 2 (2011): 95–102, https://doi.org/10.1111/j.1574-6968.2011.02295.x.

67. M. Diop, M. El-Hayek, J. Attard, et al., "Chlorophyll and Pheophytin Protonated and Deprotonated Ions: Observation and Theory," *Journal of Chemical Physics* 159, no. 19 (2023): 194308, https://doi.org/10.1063/5.0174351.

68. J. Oszmianski, J. Kolniak-Ostek, and A. Wojdyło, "Characterization and Content of Flavonol Derivatives of Allium ursinum L. Plant," *Journal of Agricultural and Food Chemistry* 61, no. 1 (2013): 176–184, https://doi.org/10.1021/jf304268e.

69. M. Ozgur, A. Akpinar-Bayizit, T. Ozcan, and L. Yilmaz-Ersan, "Effect of Dehydration on Several physico-chemical Properties and the Antioxidant Activity of Leeks (Allium Porrum L.)," *Notulae Botanicae Horti Agrobotanici Cluj-Napoca* 39, no. 1 (2011): 144–151, https://doi.org/10.15835/nbha3915861.

70. K. R. Abney, D. A. Kopsell, C. E. Sams, S. Zivanovic, and D. E. Kopsell, "UV-B Radiation Impacts Shoot Tissue Pigment Composition in Allium fistulosum L. Cultigens," *The Scientific World Journal* 2013, no. 1 (2013): 513867, https://doi.org/10.1155/2013/513867.

71. G. Liebisch, E. Fahy, J. Aoki, et al., "Update on LIPID MAPS Classification, Nomenclature, and Shorthand Notation for MS-derived Lipid Structures," *Journal of Lipid Research* 61, no. 12 (2020): 1539–1555, https://doi.org/10.1194/jlr.S120001025.

72. M. C. Tsiaganis, K. Laskari, and E. Melissari, "Fatty Acid Composition of Allium Species Lipids," *Journal of Food Composition and Analysis* 19, no. 6-7 (2006): 620–627, https://doi.org/10.1016/j.jfca.2005.06.003.

73. M. M. Elattar, H. M. Hammoda, D. A. Ghareeb, et al., "Insights into Bioactive Constituents of Onion (Allium cepa L.) Waste: a Comparative Metabolomics Study Enhanced by Chemometric Tools," *BMC Complementary Medicine and Therapies* 24, no. 1 (2024): 271, https://doi.org/10.1186/s12906-024-04559-2.

74. M. K. Huh, "Effect of Chlorophyll Content in Garlic Chives (*Allium tuberosum*) Leaves Under Drought and Ph Stress," *European Journal of Agriculture and Food Sciences* 4, no. 3 (2022): 66–69, https://doi.org/10.24018/ejfood.2022.4.3.508.

75. M. Tokoro, K. Gotoh, Y. Kudo, et al., "α-tocopherol Suppresses Hepatic Steatosis by Increasing CPT-1 Expression in a Mouse Model of diet-induced NAFLD," *Obesity Science & Practice* 7, no. 1 (2020): 91–99, https://doi.org/10.1002/osp4.460.

76. X. Qi, J. Guo, Y. Li, et al., "Vitamin E Intake Is Inversely Associated with NAFLD Measured by Transient Elastography," *Scientific Reports* 14, no. 1 (2024): 2592, https://doi.org/10.1038/s41598-024-52482-w.

77. D. Ivancovsky-Wajcman, N. Fliss-Isakov, F. Salomone, et al., "Dietary Vitamin E and C Intake is Inversely Associated with NAFLD Severity," *Digestive and Liver Disease* 51, no. 12 (2019): 1698–1705, https://doi.org/10.1016/j.dld.2019.06.005.

78. M. C. Podszun, A. S. Alawad, S. Lingala, et al., "Vitamin E Treatment in NAFLD Patients Demonstrates that Oxidative Stress Drives Steatosis Through Upregulation of De Novo Lipogenesis," *Redox Biology* 37 (2020): 101710, https://doi.org/10.1016/j.redox.2020.101710.

79. P. Wal, S. Yadav, S. K. Jha, et al., "Role of Natural Compounds in NAFLD: a Mechanistic Approach," *Egyptian Liver Journal* 15, no. 1 (2025): 50, https://doi.org/10.1186/s43066-025-00452-w.

80. G. Howell, X. Deng, C. Yellaturu, et al., "N-3 Polyunsaturated Fatty Acids Suppress insulin-induced SREBP-1c Transcription via Reduced Trans-activating Capacity of Lxrα," *Biochimica et Biophysica Acta* 1791, no. 12 (2009): 1190–1196, https://doi.org/10.1016/j.bbalip.2009.08.008.

81. L. D. Ly, S. Xu, S. K. Choi, et al., "Oxidative Stress and Calcium Dysregulation by Palmitate in Type 2 Diabetes," *Experimental & Molecular Medicine* 49 (2017): e291, https://doi.org/10.1038/emm.2016.157.

82. S. H. Kim, C. Yun, D. Kwon, Y. H. Lee, J. H. Kwak, and Y. S. Jung, "Effect of Isoquercitrin on Free Fatty acid-induced Lipid Accumulation

in HepG2 Cells," *Molecules* 28, no. 3 (2023): 1476, https://doi.org/10.3390/molecules28031476.

83. B. A. Guerra and R. Otton, "Impact of Astaxanthin on Phagocytic Capacity and ROS/RNS Production in Neutrophils Treated with Fatty Acids and High Glucose," *International Immunopharmacology* 11, no. 12 (2011): 2220–2226, https://doi.org/10.1016/j.intimp.2011.10.004.

84. J. Han and R. J. Kaufman, "The Role of ER Stress in Lipid Metabolism and Lipotoxicity," *Journal of Lipid Research* 57, no. 8 (2016): 1329–1338, https://doi.org/10.1194/jlr.R067595.

85. X. Q. Zhang, C. F. Xu, C. H. Yu, W. X. Chen, and Y. M. Li, "Role of Endoplasmic Reticulum Stress in NAFLD Pathogenesis," *World Journal of Gastroenterology* 20, no. 7 (2014): 1768–1776, https://doi.org/10.3748/wjg.v20.i7.1768.

86. C. Lebeaupin, D. Vallée, Y. Hazari, C. Hetz, E. Chevet, and B. Bailly-Maitre, "Endoplasmic Reticulum Stress Signalling and NAFLD Pathogenesis," *Journal of Hepatology* 69, no. 4 (2018): 927–947, https://doi.org/10.1016/j.jhep.2018.06.008.

87. X. Zhu, T. Xiong, P. Liu, et al., "Quercetin Ameliorates HFD-Induced NAFLD by Promoting VLDL Assembly and Lipophagy via IRE1α/XBP1s Pathway," *Food and Chemical Toxicology* 114 (2018): 52–60, https://doi.org/10.1016/j.fct.2018.02.019.

88. M. Sotiropoulou, I. Katsaros, M. Vailas, et al., "Nonalcoholic Fatty Liver Disease: the Role of Quercetin and Its Therapeutic Implications," *Saudi Journal of Gastroenterology* 27, no. 6 (2021): 319–330, https://doi.org/10.4103/sjg.sjg_249_21.

89. N. Chang, J. Li, S. Lin, et al., "Emerging Roles of the SIRT1 Activator SRT2104 in Disease Treatment," *Scientific Reports* 14, no. 1 (2024): 5521, https://doi.org/10.1038/s41598-024-55923-8.

90. A. Vikal, R. Maurya, P. Patel, and B. D. Kurmi, "Lutein as a Liver Guardian: Hepatoprotective Mechanisms, Bioavailability, and Emerging Therapeutic Roles," *Pharmacology Research & Natural Products* 9 (2025): 100387, https://doi.org/10.1016/j.prenap.2025.100387.

91. J. Winarto, D.-G. Song, and C.-H. Pan, "The Role of Fucoxanthin in Non-alcoholic Fatty Liver Disease," *International Journal of Molecular Sciences* 24, no. 9 (2023): 8203, https://doi.org/10.3390/ijms24098203.

92. H. Liu, J. Yan, F. Guan, et al., "Zeaxanthin Prevents Ferroptosis by Enhancing Mitochondrial Function and Inhibiting the p53 Pathway in FFA-Treated HepG2 Cells," *Biochimica et Biophysica Acta, Molecular and Cell Biology of Lipids* 1868, no. 4 (2023): 159287, https://doi.org/10.1016/j.bbalip.2023.159287.

93. M. Kobori, Y. Ni, Y. Takahashi, et al., "β-cryptoxanthin Alleviates diet-induced NASH by Suppressing Inflammatory Gene Expression in Mice," *PLoS One* 9, no. 5 (2014): e98294, https://doi.org/10.1371/journal.pone.0098294.

94. C. Liu, B. P. M. Rafacho, and X. D. Wang, "Xanthophyll β-cryptoxanthin Treatment Inhibits Hepatic Steatosis Without Altering Vitamin A Status in BCO2-deficient Mice," *Hepatobiliary Surgery and Nutrition* 11, no. 2 (2022): 188–198, https://doi.org/10.21037/hbsn-20-404.

Supporting Information

Additional supporting information can be found online in the Supporting Information section. **Supporting Information.** Figure S1. Chlorophyll and carotenoid contents in the CN extract; Figure S2. Cell viability was examined by the MTT assay; Figure S3. Cell viability of the CN extract examined by the MTT assay; Table S1. Parameters used in the Compound Discoverer Workflow; Table S2. Parameters set in MZmine-mzwizard workflow.